Monthly Notices of the ROYAL ASTRONOMICAL SOCIETY

MNRAS **536,** 554–571 (2025) https://doi.org/10.1093/mnras/stae2567
Advance Access publication 2024 November 15

Radio-AGN activity across the galaxy population: dependence on stellar mass, star formation rate, and redshift

Rohit Kondapally [1]★ Philip N. Best,[1] Kenneth J. Duncan [1] Huub J. A. Röttgering,[2] Daniel J. B. Smith [3] Isabella Prandoni [4] Martin J. Hardcastle [3] Tanja Holc,[1] Abigail L. Patrick,[1] Marina I. Arnaudova [3] Beatriz Mingo [3,5] Rachel K. Cochrane [1,6] Soumyadeep Das [3] Paul Haskell,[3] Manuela Magliocchetti [7] Katarzyna Małek,[8] George K. Miley,[2] Cyril Tasse[9,10] and Wendy L. Williams[11]

[1]*Institute for Astronomy, University of Edinburgh, Royal Observatory, Blackford Hill, Edinburgh EH9 3HJ, UK*
[2]*Leiden Observatory, Leiden University, PO Box 9513, NL-2300 RA Leiden, the Netherlands*
[3]*Centre for Astrophysics Research, University of Hertfordshire, College Lane, Hatfield AL10 9AB, UK*
[4]*INAF–Istituto di Radioastronomia, Via Gobetti 101, I-40129 Bologna, Italy*
[5]*School of Physical Sciences, The Open University, Walton Hall, Milton Keynes MK7 6AA, UK*
[6]*Department of Astronomy, Columbia University, New York, NY 10027, USA*
[7]*INAF–IAPS, Via Fosso del Cavaliere 100, I-00133 Rome, Italy*
[8]*National Centre for Nuclear Research, Pasteura 7, PL-02-093 Warsaw, Poland*
[9]*GEPI & ORN, Observatoire de Paris, Université PSL, CNRS, 5 Place Jules Janssen, F-92190 Meudon, France*
[10]*Department of Physics & Electronics, Rhodes University, PO Box 94, Grahamstown 6140, South Africa*
[11]*SKA Observatory, Jodrell Bank, Lower Withington, Macclesfield SK11 9FT, UK.*

Accepted 2024 November 11. Received 2024 October 28; in original form 2024 August 30

ABSTRACT

We characterize the co-evolution of radio-loud active galactic nuclei (AGN) and their galaxies by mapping the dependence of radio-loud AGN activity on stellar mass and star formation rate (SFR) across cosmic time (out to $z \sim 1.5$). Deep LOFAR radio observations are combined with large galaxy samples to study the incidence of radio-loud AGN across the galaxy population; the AGN are further split into low-excitation radio galaxies (LERGs) and high-excitation radio galaxies (HERGs). We find that LERG activity occurs over a wide range of SFRs, whereas HERGs are typically found in galaxies with ongoing star formation. The LERGs are then split based on their SFRs relative to the main sequence, across redshift. Within quiescent galaxies, LERG activity shows a steep stellar mass dependence with the same normalization across the past ∼10 Gyr; this indicates that hot gas fuels LERGs in quiescent galaxies across cosmic time. In massive galaxies [$\log_{10}(M/\mathrm{M}_{\odot}) \gtrsim 11$], the incidence of LERGs is roughly constant across the galaxy population, suggesting that LERGs in massive galaxies may be fuelled by hot gas regardless of the star formation activity. At lower masses, however, LERG activity is significantly more enhanced (by a factor of up to 10) in star-forming galaxies compared to quiescent galaxies; this suggests that an additional fuelling mechanism, likely associated with cold gas, may fuel the LERGs in galaxies with higher SFRs. We find that HERGs typically accrete above 1 per cent of the Eddington-scaled accretion rate, and the LERGs typically accrete below this level.

Key words: galaxies: active – galaxies: evolution – galaxies: jets – radio continuum: galaxies.

1 INTRODUCTION

It is now widely believed that supermassive black holes (SMBHs) and their host galaxies co-evolve across cosmic time, with evidence for a link between the build-up of stars and the growth of the SMBHs (e.g. Kormendy & Ho 2013), and a tight correlation between the mass of the SMBH and that of the galaxy bulge component (e.g. Ferrarese & Merritt 2000; Merritt & Ferrarese 2001). SMBHs can undergo an active phase, powered by accretion of matter on to the black hole, during which they are referred to as active galactic nuclei (AGN). These AGN can emit vast amounts of energy across the electromagnetic spectrum in the form of ionizing outflows or relativistic jets, which can suppress or regulate subsequent star formation within the host galaxy; this is referred to as AGN feedback (e.g. Best et al. 2005b; Cattaneo et al. 2009; Fabian 2012; Heckman & Best 2014; Hardcastle & Croston 2020). AGN feedback is often invoked in cosmological simulations to suppress the growth of the most massive haloes and reproduce the observed local galaxy luminosity functions (e.g. Bower et al. 2006; Croton et al. 2006; Somerville & Davé 2015).

Of particular importance in the lifecycle of massive galaxies and clusters are radio-loud AGN (hereafter; radio-AGN), which emit powerful bipolar jets of relativistic ionized material that radiate syn-

★ E-mail: rohitkondapally@gmail.com

chrotron emission, which is visible at radio wavelengths. The energy deposited by these radio-jets into the host galaxy and surrounding environment can balance the radiative cooling losses and regulate star formation in massive galaxies, with recurrent radio-AGN heating required to 'maintain' galaxies as 'red and dead' once quenched, in the nearby Universe (see Best et al. 2006, 2007; McNamara & Nulsen 2007; Heckman & Best 2014; Hardcastle & Croston 2020).

Radio-AGN are typically classified into two modes, based on the nature of the emission lines in their optical spectra, as low-excitation radio galaxies (LERGs) and high-excitation radio galaxies (HERGs). This classification is understood to be linked to the nature of the accretion flow on to the SMBH (see Best et al. 2005a; Allen et al. 2006; Hardcastle, Evans & Croston 2007; Hardcastle 2018), where HERGs are associated with radiatively efficient accretion, typically from cold gas, which leads to the formation of a geometrically thin, optically thick accretion disc, and a dusty torus (e.g. Shakura & Sunyaev 1973); as a result, they display high-excitation emission lines due to photoionization of gas from accretion disc photons. In contrast, LERGs are associated with a radiatively inefficient accretion flow (e.g. Narayan & Yi 1994, 1995; Yuan & Narayan 2014), often modelled as arising from cooling hot gas, and as a result, do not display signs of a typical AGN such as an optically thick accretion disc or a torus, and therefore lack high-excitation emission lines in their optical spectra. In this scenario, the HERGs have been argued to typically accrete at $\gtrsim$1 per cent of the Eddington-scaled accretion rate, whereas the LERGs accrete at much lower rates of $\lesssim$1 per cent of the Eddington-scaled accretion rate (Best & Heckman 2012; Mingo et al. 2014).

Studies of LERGs and HERGs in the nearby Universe have also shown differences in host galaxy properties between the two classes. LERGs are typically found to be hosted in massive, quiescent, red galaxies with massive black holes, and are often found in rich group or cluster environments, whereas HERGs tend to be found in less-massive galaxies, with recent or on-going star formation, and in poorer environments (e.g. Tasse et al. 2008; Smolčić et al. 2009; Best & Heckman 2012; Gendre et al. 2013; Sabater, Best & Argudo-Fernández 2013; Mingo et al. 2014; Williams & Röttgering 2015; Ching et al. 2017; Williams et al. 2018; Croston et al. 2019; Magliocchetti 2022). Although both LERGs and HERGs are found across a wide range of luminosities, the characteristic break in the luminosity function for HERGs occurs at higher luminosities, and they are found to also show a stronger space density evolution with redshift (e.g. Best & Heckman 2012; Best et al. 2014; Pracy et al. 2016; Butler et al. 2019; Kondapally et al. 2022). These observed properties of the host galaxies of LERGs and HERGs can be understood in terms of the different accretion properties of these AGN. The cooling of hot gas within massive, quiescent galaxies is expected to lead to low-accretion rates resulting in the formation of a LERG, whereas the plentiful supply of cold gas present in lower mass, star-forming systems may also lead to higher accretion rates, resulting in a HERG.

Using deep observations from the Low Frequency ARray (LOFAR) Two-metre Sky Survey Deep Fields Data Release 1 (LoTSS-Deep DR1; Duncan et al. 2021; Kondapally et al. 2021; Sabater et al. 2021; Tasse et al. 2021; Best et al. 2023), Kondapally et al. (2022) studied the cosmic evolution of LERGs, finding that at $z \gtrsim 1$, most of the LERGs are hosted by star-forming galaxies (SFGs), in contrast to studies at lower redshifts where LERGs are predominantly found in quiescent galaxies (e.g. Best & Heckman 2012). These results suggest that there may be differences in the host galaxy properties of AGN in the early Universe and at lower luminosities, with some overlap with the host galaxy properties of HERGs (see also Whittam et al. 2018, 2022). Moreover, the significant population of LERGs hosted in a different galaxy type (star-forming as opposed to quiescent) at early times can have interesting implications for both the fuelling mechanisms (see also Delvecchio et al. 2022) and our current understanding of AGN feedback processes and its effect on the galaxy population (e.g. Cattaneo et al. 2009; Smolčić et al. 2017b; Butler et al. 2019; Hardcastle & Croston 2020; Kondapally et al. 2023; Heckman et al. 2024).

It is well known that in the local Universe, the fraction of galaxies hosting a radio-AGN (which provides a measure of the duty cycle) strongly increases with stellar mass as $f_{\rm radio-AGN} \propto M_{\star}^{2.5}$ (Best et al. 2005a; Smolčić et al. 2009), with recent work by Sabater et al. (2019) finding that at low luminosities almost all massive galaxies host a radio-AGN. Janssen et al. (2012) studied the dependence of radio-AGN activity on galaxy properties at $z < 0.3$ using the radio-AGN sample of Best & Heckman (2012). Using this sample, Janssen et al. (2012) measured the incidence of LERGs and HERGs, separately, as a function of stellar mass at $z < 0.3$, finding that LERG activity increases steeply with stellar mass, consistent with $M_{\star}^{2.5}$, whereas the HERGs showed a much shallower dependence of $\propto M_{\star}^{1.5}$. Moreover, they found that compared to red galaxies, HERG activity was significantly more enhanced in blue galaxies at fixed stellar mass. These results are consistent with the notion of LERGs undergoing accretion from cooling of hot gas within massive haloes, with the HERGs being fuelled by the abundant cold gas present in their lower mass (bluer), star-forming host galaxies (e.g. Best et al. 2005a).

Early and recent works that extended this analysis out to higher redshifts have found a similarly steep stellar mass dependence for the entire radio-AGN population (e.g. Tasse et al. 2008; Smolčić et al. 2009; Simpson et al. 2013; Williams & Röttgering 2015; Williams et al. 2018; Igo et al. 2024; Wang et al. 2024). Since the radio-AGN population consists of both the LERGs and HERGs, Kondapally et al. (2022) used data from one of the LoTSS Deep Fields to study how the incidence of LERGs, alone, depends on stellar mass within quiescent and SFGs, separately, to $z \sim 1.5$. They found that LERGs hosted by quiescent galaxies showed a redshift-invariant steep stellar mass dependence, highly consistent with observations in the local Universe of fuelling occurring from cooling hot gas (see also Williams et al. 2018). On the other hand, the LERGs hosted by SFGs showed a much shallower dependence on stellar mass, suggesting that LERGs in more star-forming systems may be fuelled in a manner different from those in quiescent galaxies.

In this paper, we aim to extend these analyses to understand how radio-AGN are triggered across the galaxy population by measuring the incidence of these radio-AGN as a function of each of stellar mass, star formation rate (SFR), and redshift; using the full LoTSS Deep Fields data set allows us to split our sample across these parameters simultaneously. This paper is structured as follows. Section 2 describes the radio and multiwavelength data set, along with the selection of radio-AGN and the parent sample used for comparison. Section 3 presents the results on the incidence of LERGs and HERGs as a function of mass and SFR. In Section 4, we present the results on the dependence of LERG activity as a function of SFR relative to the main sequence of star formation. In Section 5, we present the Eddington-scaled accretion rate properties of the LERGs and HERGs. In Section 6, we present the interpretation and discussion of our results. Section 7 presents the conclusions of our study. Throughout this work, we use a flat ΛCDM cosmology with $\Omega_{\rm M} = 0.3$, $\Omega_{\Lambda} = 0.7$ and $H_0 = 70$ km s^{-1} Mpc^{-1}, and a radio spectral index $\alpha = -0.7$ (where $S_{\nu} \propto \nu^{\alpha}$).

2 DATA

2.1 Radio and other multiwavelength data

The radio data set used in this analysis comes from LoTSS-Deep DR1 (Sabater et al. 2021; Tasse et al. 2021), based on LOFAR High Band Antenna (HBA) observations ranging from ∼113 to 177 MHz.[1] The LoTSS-Deep DR1 consists of repeated observations of the ELAIS-N1, Lockman Hole, and Boötes fields, totalling 168, 112, and 80 h, and reaching an rms sensitivity of 20, 22, and 32 μJy beam^{-1} near the centre of each field, respectively. Radio source catalogues were extracted out to the 30 per cent power point of the primary beam in each field using Python Blob Detector and Source Finder (PYBDSF; Mohan & Rafferty 2015) as detailed by Tasse et al. (2021) and Sabater et al. (2021).

The three fields benefit from extensive deep, wide-area multiwavelength imaging, including photometry from the ultraviolet, optical, near and mid-infrared, and far-infrared wavelengths provided by a suite of ground and space-based imaging surveys over the past two decades; the full details of the available multiwavelength imaging data set are described by Kondapally et al. (2021). Using this multiwavelength data set, multiband forced, matched-aperture photometry catalogues were generated in ELAIS-N1 and Lockman Hole (Kondapally et al. 2021). In the Boötes field, an adapted version of the point spread function matched catalogues from Brown et al. (2007, 2008) were used. Photometric redshifts for the multiband catalogues were determined by Duncan et al. (2021) using a hybrid method which combined standard template-fitting methods with machine-learning methods (see Duncan et al. 2018a, b). For a small fraction of sources in each field, spectroscopic redshifts were available (∼5, 5, and 20 per cent in ELAIS-N1, Lockman Hole, and Boötes, respectively) and were used instead.

The host galaxy identification process was then carried out for the LOFAR detected sources using these multiband catalogues as detailed by Kondapally et al. (2021). In summary, host galaxy counterparts were identified using the likelihood ratio (LR) method (de Ruiter, Willis & Arp 1977; Sutherland & Saunders 1992) for suitable sources (typically compact sources with well-defined positions), or otherwise using a visual classification scheme where identifications and radio-source associations were performed using consensus decisions from members of the LOFAR collaboration (see also Williams et al. 2019). This source-association and cross-matching process resulted in a catalogue of 81 951 radio sources with host galaxies identified for >97 per cent of these. Overall, the LR method was used to identify counterparts for ∼83 per cent of the sources, with a reliability and completeness of over 99 per cent, with the remaining 14 per cent of sources being classified visually (see Kondapally et al. 2021 for further details). In this paper, we restrict our analysis to sources within the redshift range $0.3 < z \leq 1.5$. We exclude sources with $z < 0.3$ as the aperture-corrected photometry, and hence the derived photometric redshifts, may not be as robust due to the extended nature of sources, while sources above $z = 1.5$ are excluded as the photometric redshifts for galaxy-dominated sources become less reliable beyond this redshift (see Duncan et al. 2021).

2.2 Identification of AGN

Spectral energy distribution (SED) fitting can be used not only to derive galaxy properties (such as stellar masses, SFRs, etc.) but also to identify and characterize AGN activity (e.g. Calistro Rivera et al. 2016; Leja et al. 2017; Boquien et al. 2019; Das et al. 2024). Best et al. (2023) performed SED fitting for the radio-detected sources in LoTSS-Deep DR1 to broadly classify them into SFGs and the different types of AGN. Deep radio continuum surveys are expected to detect a variety of source populations; a combination of different SED fitting codes that can model AGN emission and those that allow a better sampling of normal galaxies (i.e. those without an AGN component) were used by Best et al. (2023) to optimize the classification process. In summary, for each radio source, using the best-estimate redshift (photometric or spectroscopic if available), SED fitting was performed using each of AGNFITTER (Calistro Rivera et al. 2016), BAGPIPES (Carnall et al. 2018), CIGALE (Burgarella, Buat & Iglesias-Páramo 2005; Noll et al. 2009; Boquien et al. 2019), and MAHPHYS (da Cunha, Charlot & Elbaz 2008). Both AGNFITTER and CIGALE, unlike the other two codes, employ models for fitting the emission from the AGN accretion disc and torus which can result in more robust fits of physical properties for galaxies hosting an AGN, while also allowing the identification of AGN.

Best et al. (2023) began by identifying radiative-mode AGN using the outputs from the four SED fitting codes. First, using the results from AGNFITTER and CIGALE, they defined a parameter $f_{\rm AGN,16}$ (from each code) which represents the 16th percentile of the fraction of the total mid-infrared luminosity arising from AGN components. Then, the reduced χ^2 values from AGNFITTER and CIGALE, which model AGN emission, were compared to the reduced χ^2 values from BAGPIPES and MAGPHYS; for sources with infrared AGN emission, the former two codes should find a better SED fit. The combination of these two criteria were primarily used to identify the radiative-mode AGN (see Best et al. 2023 for the exact criteria employed). In addition to the above, for ELAIS-N1 and Lockman Hole, bright X-ray detected AGN were identified using the Second *ROSAT* All-Sky Survey (2RXS; Boller et al. 2016) and the *XMM–Newton* Slew Survey (XMMSL2).[2] In Boötes, deep, wide-area observations from the X-Boötes survey (Kenter et al. 2005) were used to identify AGN (see Duncan et al. 2021). In addition, for a small fraction of the sources, optical spectroscopy indicated the presence of an AGN, which were also classified as radiative-mode AGN. The final list of radiative-mode AGN were comprised of those classified from the Best et al. SED fitting, plus a small fraction of additional X-ray or spectroscopically selected AGN that were not already identified from the SED fits. For sources classified as radiative-mode AGN, the 'consensus' SFRs and stellar masses were primarily derived using the CIGALE output (as BAGPIPES and MAGPHYS may be unreliable as they did not model the AGN component and AGNFITTER was found to result in larger uncertainties in general). For sources not classified as radiative-mode AGN, consensus SFRs and stellar masses were estimated using the mean of the values from BAGPIPES and MAGPHYS (provided an acceptable fit was found in each case) as these are expected to be most reliable in the absence of AGN activity due to their sampling of galaxy parameters. Throughout the analysis in this paper, we use these consensus SFRs and stellar masses for our radio-AGN sample.

A tight-correlation is observed between radio-luminosity and SFR for SFGs (e.g. Calistro Rivera et al. 2016; Gürkan et al. 2018; Smith et al. 2021; Das et al. 2024), which can be used to identify radio-loud AGN as sources that show a significant radio-luminosity excess (also known as 'radio-excess' AGN) relative to this relation (e.g. Delvecchio et al. 2017; Smolčić et al. 2017a;

[1] We refer to the central frequency throughout this paper as 150 MHz, for simplicity.

[2] https://www.cosmos.esa.int/web/xmm-newton/xmmsl2-ug

Williams et al. 2018; Whittam et al. 2022). Following this, Best et al. (2023) used a 'ridgeline' approach, which is well-fitted by $\log_{10}(L_{150\,\mathrm{MHz}}/\mathrm{W\,Hz^{-1}}) = 22.24 + 1.08\log_{10}(\mathrm{SFR}/\mathrm{M_\odot\,yr^{-1}})$, to select radio-excess AGN as sources that showed a radio-excess of > 0.7 dex ($\approx 3\sigma$) compared to that expected from star formation alone.

In this study, HERGs are identified as the radiative-mode AGN that also display a radio-excess AGN. LERGs do not display signs of typical AGN accretion disc or torus features and are identified by the presence of radio-jets only; these sources are therefore selected as sources that show a radio-excess AGN but are not classified as radiative-mode AGN. In total, across the redshift range $0.3 < z \leq 1.5$, there are 38 915 radio-detected sources, of which 7530 are radio-excess AGN, which are further split into 6775 LERGs and 755 HERGs.

2.3 Potential incompleteness of radio-excess AGN at high star formation rates

The use of a radio-excess criterion in selecting radio-AGN may miss low-luminosity AGN, which may potentially bias our subsequent analysis. In particular, for sources with a given jet (AGN) luminosity, it will be more difficult to identify AGN using their radio-excess in more highly SFGs, leading to some incompleteness of radio-excess AGN at high SFRs. This may introduce a bias to our results, in conjunction with the application of a radio luminosity limit ($L_{150\,\mathrm{MHz}} \geq 10^{24}\,\mathrm{W\,Hz^{-1}}$; see Section 3). The potential impact of this selection effect on our results could be mitigated by imposing a higher radio luminosity limit, however, this would result in poorer statistics and limit our sample to only the most luminous radio-AGN whose results may not be applicable to the broader radio-AGN population. In this paper, we instead perform Monte Carlo simulations to assess and correct for the impact of this selection effect on our results; these are described in detail in Appendix A. In summary, we simulate the total 150 MHz radio luminosity of sources as arising from the sum of a star formation component and an AGN (jet) component, while accounting for the radio-luminosity–SFR relation and its scatter. The fraction of the simulated sources that would satisfy the radio-excess criterion of Best et al. (2023) was calculated to determine the completeness in narrow bins in radio luminosity and SFR. For each SFR bin, the completeness was weighted by the luminosity functions of various AGN types used in this study, down to the luminosity limit of $L_{150\,\mathrm{MHz}} \geq 10^{24}\,\mathrm{W\,Hz^{-1}}$ to compute the completeness corrections for the radio-excess selection. The output of this analysis is a set of completeness corrections as a function of SFR for different types of AGN (see Fig. A2). The results of this simulation show that our sample is consistent with 100 per cent completeness at SFR $\lesssim 10\,\mathrm{M_\odot\,yr^{-1}}$, with this decreasing steeply at higher SFRs. The completeness corrections derived from these simulations are used for further analysis in Sections 3 and 4.

2.4 Mid-infrared flux-selected parent sample

To place the properties of the radio-AGN within the broader context of the galaxy population, one must compare to a sample of underlying/parent galaxies. The parent sample used for this comparison comes from the *Spitzer* InfraRed Array Camera (IRAC) 3.6 μm flux selected ($F_{3.6\mu\mathrm{m}} > 10$ μJy) sample taken from the multiwavelength catalogues of Kondapally et al. (2021); SED fitting for this sample was performed using MAGPHYS by Smith et al. (2021) to derive stellar masses and SFRs. Smith et al. (2021) presented these results only for the ELAIS-N1 field (the deepest of the LoTSS Deep Fields), however this process was subsequently repeated for both the Lockman Hole and Boötes fields (Smith et al. private communication) using similar input multiwavelength photometry catalogues from Kondapally et al. (2021) which we use in this study. As noted by Duncan et al. (2021), the photometric redshifts for galaxy-dominated (rather than AGN-dominated) systems in the three LoTSS Deep Fields are found to be most robust out to $z \sim 1.5$, and therefore the SED fitting process for the IRAC-selected sample (and therefore for the LoTSS-Deep sample), and further analysis in this paper is also limited to $z \leq 1.5$. In total, across the redshift range $0.3 < z \leq 1.5$, there are 540 279 sources in the parent IRAC-selected sample. Throughout this analysis, this parent mid-infrared (MIR) flux selected sample (and the resulting physical properties such as SFRs and stellar masses) is used for comparison with the LoTSS-Deep radio-AGN sample. As shown by Best et al. (2023), the stellar masses and SFRs derived for the parent sample, although using a slightly different method compared to the LoTSS Deep sources, are consistent.

Throughout the analysis in this paper, we compare the properties of the radio-AGN as a function of their stellar mass. For this analysis, it is important to account for mass incompleteness in our sample to avoid any biases in the interpretation of our results. We use the stellar mass completeness limits determined by Duncan et al. (2021) for the underlying multiwavelength data set which was used to identify the host galaxies of the radio sources and forms the basis of the mid-infrared parent sample. Duncan et al. (2021) determined the 90 per cent stellar mass completeness limits as a function of redshift by accounting for a maximally old stellar population, ensuring a complete sample of quiescent galaxies for each of the three LoTSS Deep fields, separately. Using these completeness limits, in the analysis throughout the rest of this paper, we estimate the mass above which a source would be detected over an entire chosen redshift range and remove sources (from both the radio-AGN and the mid-infrared parent sample) below this mass limit from the analysis.

3 THE INCIDENCE OF RADIO-AGN ACTIVITY ON STELLAR MASS AND SFR

In Fig. 1, we present the cosmic evolution of the fraction of all galaxies that host a LERG (*left*) or a HERG (*right*) as a function of stellar mass for a radio luminosity limit of $L_{150\,\mathrm{MHz}} \geq 10^{24}\,\mathrm{W\,Hz^{-1}}$. The results are calculated across five redshift bins ($0.3 < z \leq 0.5$, $0.5 < z \leq 0.7$, $0.7 < z \leq 1.0$, $1.0 < z \leq 1.2$, and $1.2 < z \leq 1.5$), shown by the different colours. The error bars are calculated following binomial statistics. The chosen radio luminosity limit of $L_{150\,\mathrm{MHz}} \geq 10^{24}\,\mathrm{W\,Hz^{-1}}$ corresponds to a 5σ detection limit (based on the depth of the deepest field) for a source out to $z \sim 1.5$; moreover, this 150 MHz radio luminosity limit is also comparable to the 1.4 GHz radio luminosity limit of $10^{23}\,\mathrm{W\,Hz^{-1}}$ often used in the literature for similar studies (e.g. Best et al. 2005a; Janssen et al. 2012), given the typical radio spectral index (assuming $\alpha \approx -0.7$). There are 3525 LERGs and 412 HERGs that satisfy the above radio luminosity limit across the chosen redshift range for our analysis. In the left panel for the LERGs, the black dashed line represents the fraction of galaxies hosting a LERG at a given stellar mass, f_{LERG}, found in the local Universe, given as $f_{\mathrm{LERG}} = 0.01\left(M_\star/10^{11}\,\mathrm{M_\odot}\right)^{2.5}$ (Best et al. 2005a; Janssen et al. 2012); this relation has been roughly normalized based on these low-redshift results but we note that the precise normalization depends on the radio luminosity limit and hence on the assumed spectral index. In the right panel, the black dotted line corresponds to the shallower stellar mass dependence found

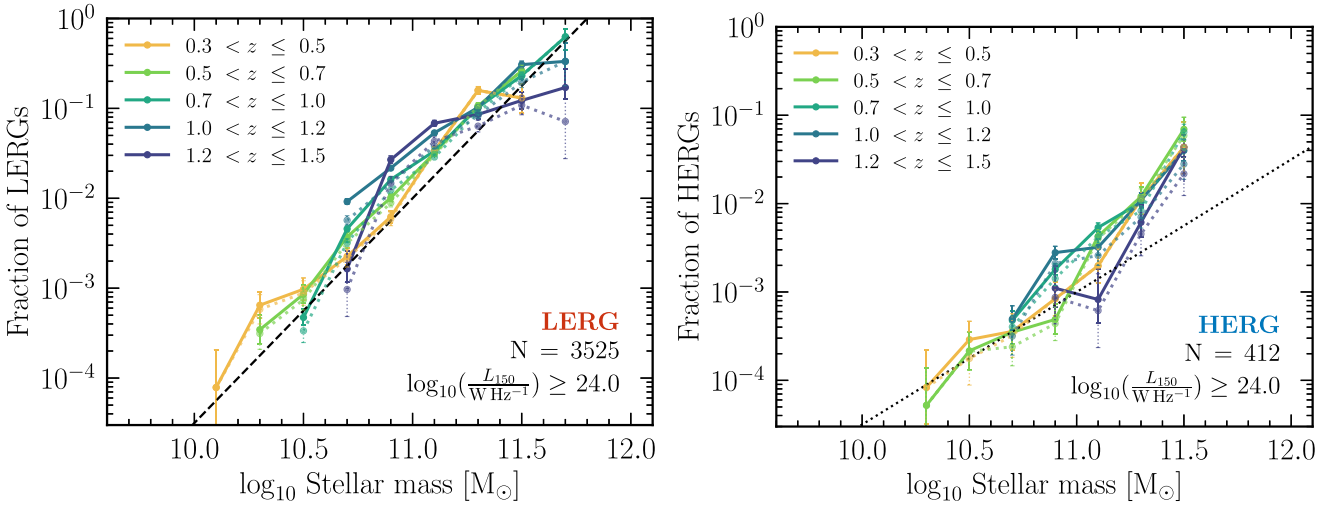

Figure 1. The fraction of all galaxies that host a LERG (*left*) or a HERG (*right*) as a function of stellar mass across $0.3 < z \leq 1.5$ for a radio-luminosity limit of $L_{150\,\mathrm{MHz}} \geq 10^{24}\,\mathrm{W\,Hz^{-1}}$. The numbers of LERGs and HERGs satisfying the radio-luminosity limit over this redshift range are also listed in each panel. The solid and dotted lines show the fractions obtained with and without the radio-luminosity–SFR completeness corrections, respectively (see the text and Appendix A); these corrections have a small effect for the overall populations. The black dashed line in the left panel represents the steep stellar mass relation ($\propto M_\star^{2.5}$, normalized to 0.01 at $M = 10^{11}\,\mathrm{M}_\odot$) found for LERGs in the local Universe (Best et al. 2005a; Janssen et al. 2012). The black dotted line in the right panel corresponds to the shallow mass dependence ($\propto M_\star^{1.5}$, normalized to 0.001 at $M = 10^{11}\,\mathrm{M}_\odot$), similar to that found for HERGs in the local Universe (Janssen et al. 2012). The LERGs show the same steep relation as observed in the local Universe all the way out to $z \sim 1.5$. The HERG fraction at low masses follow a shallower relation at $M < 10^{11}\,\mathrm{M}_\odot$, but show a steeper than expected relation (based on higher frequency local Universe studies) at higher masses.

for HERGs in the local Universe ($\propto M_\star^{1.5}$; Janssen et al. 2012), which has been scaled to correspond to $f_{\mathrm{HERG}} = 0.001\,\left(M_\star/10^{11}\,\mathrm{M}_\odot\right)^{1.5}$.

As noted in Section 2.3, we have derived completeness corrections to account for radio-excess selection effects, which are detailed in Appendix A; this analysis indicates that we achieve a lower completeness of radio-excess AGN at higher SFRs. For each stellar mass bin, we apply the corrections (for the LERGs and HERGs, separately) shown in Fig. A2. For each redshift bin in Fig. 1, the solid and dotted lines show the fractions with and without these completeness corrections applied, respectively. Applying this correction increases the fraction of galaxies hosting a LERG or a HERG, which is noticeable as we tend toward high-stellar masses and high redshifts, where the average SFRs increase. For the LERGs, these corrections only significantly affect the most massive systems within the highest redshift bin in Fig. 1, however the data points with and without the corrections are consistent within their uncertainties. For the HERGs, small differences are seen across a wider range of stellar masses and redshifts. This suggests that the completeness corrections have a small effect on the stellar mass dependencies, particularly at high masses and redshifts.

The results from Fig. 1 for the LERGs show that the incidence of LERGs has a steep stellar mass dependence out to $z \sim 1.5$. The dependence on stellar mass appears to slightly flatten with increasing redshift, as previously shown by Kondapally et al. (2022) for the LERGs and by Williams & Röttgering (2015) for the total radio-AGN population. We note that the requirement of high black hole masses ($\mathrm{M_{BH}} > 10^{7.8}\,\mathrm{M}_\odot$) to launch powerful radio jets found by Whittam et al. (2022) is consistent with the high prevalence of LERG activity in the most massive galaxies observed in this study. Broadly the results for the LERG population are consistent with studies in the local Universe (e.g. Best et al. 2005a; Tasse et al. 2008; Janssen et al. 2012; Sabater et al. 2019), with some evidence of flattening at lower masses and higher redshifts, which we investigate further in Section 4. The dependence of HERG activity on stellar mass shows different trends compared to local Universe studies. At $\log_{10}(M_\star/\mathrm{M}_\odot) \lesssim 11$, the HERGs trace the slope of the black dotted line well, which corresponds to the shallow $\propto M_\star^{1.5}$ dependence observed in the local Universe, albeit with a higher normalization by a factor of $\sim$ 2–3 at a given stellar mass. Janssen et al. (2012) also studied the HERG fractions when split by those hosted by blue galaxies alone; their normalization of the HERG fractions within blue galaxies agrees well with our results for the total HERG population shown here. At higher masses, and also with increasing redshift, our results indicate a steeper mass dependence, with a higher prevalence of HERGs in massive galaxies than expectations from low redshift studies.

The HERG population is known to exhibit strong evolution with redshift (e.g. Best et al. 2014; Pracy et al. 2016; Williams et al. 2018; Kondapally et al. 2022); some of the observed differences with our study could be due to cosmic evolution, since even the lowest redshift bin in this study probes earlier epochs than the typical redshift of the Janssen et al. (2012) sample of $z_{\mathrm{med}} \sim 0.15$. Another source of differences could arise from the different source classification methods used to identify LERGs and HERGs. Janssen et al. (2012) used spectroscopic classifications by Best & Heckman (2012) based on emission line ratio diagnostics to identify LERGs and HERGs; this is typically considered to be the 'gold standard' method of classifying radiatively efficient versus inefficient accretion. In this paper, we do not have spectroscopic information available for the vast majority of the radio sources, therefore SED fitting is used for the classification instead (see Section 2.2). It is possible that a small fraction of LERGs mis-classified as HERGs could cause an increase in the AGN fraction of HERGs, particularly at high masses where the LERG fraction is $\sim$10 per cent. We discuss the potential uncertainties in our source classification method in Section 5.1 and further validate the robustness of this in Appendix B.

We investigate the dependence of radio-AGN activity on star formation activity in Fig. 2, which shows the fraction of galaxies that host a LERG (lower left) or a HERG (lower right) as a

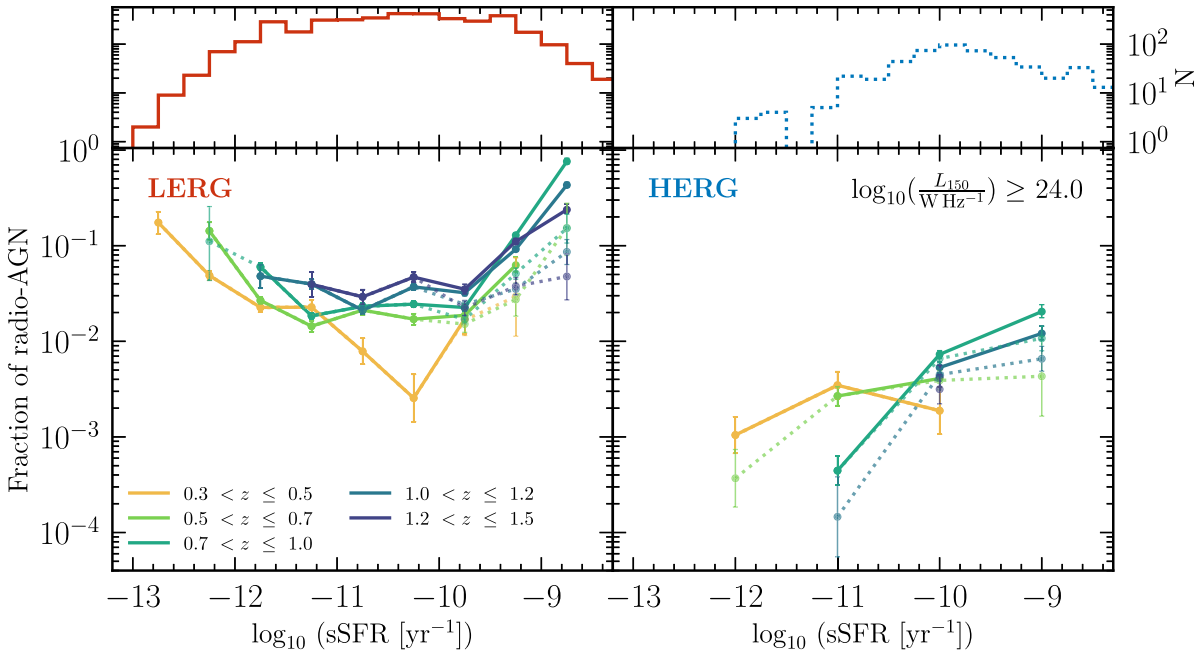

Figure 2. The fraction of galaxies that host a LERG (*lower left*) or a HERG (*lower right*) with $L_{150\,\mathrm{MHz}} \geq 10^{24}\,\mathrm{W\,Hz^{-1}}$ as a function of sSFR across $0.3 < z \leq 1.5$. To reduce any mass selection effects, we calculate the fractions for a constant stellar mass range of $10.8 < \log_{10}(M_\star/\mathrm{M}_\odot) \leq 11.5$ (see the text) across the redshift bins. The solid and dotted lines show the results with and without the radio-luminosity–SFR completeness correction (see Section 2.3). The corresponding top panels on the left and right show the distribution of the sSFRs for the LERGs and HERGs, respectively. The LERGs show a broad sSFR distribution, whereas the HERGs tend to be preferentially hosted in SFGs. For the LERGs, the radio-AGN fraction remains mostly flat across many orders of magnitude in sSFR, only increasing above $\log_{10}(\mathrm{sSFR/yr^{-1}}) \gtrsim -10$.

function of their specific SFR ($\mathrm{sSFR} = \mathrm{SFR}/\mathrm{M}_\star$) for AGN with $L_{150\,\mathrm{MHz}} \geq 10^{24}\,\mathrm{W\,Hz^{-1}}$. The analysis is performed out to $z \sim 1.5$ over the same redshift bins as in Fig. 1. To ensure the results are not biased by selection effects across different redshift bins, we restrict this analysis to sources with $10.8 < \log_{10}(M_\star/\mathrm{M}_\odot) \leq 11.5$; the lower limit is chosen to roughly corresponds to the 90 per cent stellar mass completeness limit at $z = 1.5$. As in Fig. 1, the solid and dotted lines show the results with and without the radio-excess completeness corrections applied, respectively (see Appendix A). The uncertainties are calculated following binomial statistics. The top panels show the corresponding distributions of the sSFRs for the LERGs and HERGs.

The fraction of galaxies hosting a LERGs reaches $\gtrsim$10 per cent in the most quiescent galaxies (i.e. at the lowest sSFRs), before declining to a few per cent level across $-12 < \log_{10}(\mathrm{sSFR/yr^{-1}}) < -10$. At higher sSFRs, for the most star-forming systems, the LERG fraction shows a strong increase; this trend is seen across redshift out to $z \sim 1.5$. We note the dip in the fraction at intermediate sSFRs at $z \leq 0.5$ is only at a $\approx 2\sigma$ level with a small number of sources. Our results for the LERGs show that their hosts span a broad range of star formation activities and that the prevalence remains broadly constant across a wide range of sSFRs; we investigate the trends with star formation activity in more detail in Section 4. The HERGs show a much lower prevalence than the LERGs at all sSFRs, similar to the stellar mass dependence results shown in Fig. 1. The results in Fig. 2 show that HERGs are more likely to be found in star-forming systems compared to quiescent systems, albeit with relatively small numbers of HERGs in each bin resulting in large statistical uncertainties. These findings for the HERGs are in good agreement with previous studies (e.g. Best & Heckman 2012; Best et al. 2014; Mingo et al. 2014; Pracy et al. 2016).

4 DEPENDENCE OF RADIO-AGN ACTIVITY ON SFR RELATIVE TO THE MAIN SEQUENCE

In this section, we explore the properties of the LERGs in more detail by studying the incidence of LERGs as a function of their position relative to the star-forming main sequence. As the HERGs are typically found to be hosted in star-forming systems and given the relatively small numbers of HERGs observed, performing detailed statistical analyses for the HERGs as a function of SFR and stellar mass, simultaneously, is not feasible; we therefore focus our further analysis in this section on the LERGs alone.

We divide our AGN and galaxy samples into three sub-groups based on their SFR relative to the star-forming main sequence: quiescent, intermediate, and star-forming. For this, we use the best-fitting relation for the star-forming main sequence from Speagle et al. (2014), which was found to provide a good fit to the observed SFRs out to $z \sim 5$, given as

$$\log_{10}(\mathrm{SFR_{MS}}(t)) = (0.84 - 0.026 \times t)\log_{10}(M_\star) - 6.51 + 0.11 \times t, \quad (1)$$

where $\mathrm{SFR_{MS}}$ is the main-sequence SFR (in $\mathrm{M_\odot\,yr^{-1}}$ units) and t is the age of the Universe at z. Using this, we split our sample into three regions along the SFR $-$ $\mathrm{M}_\star$ plane as follows:

(i) 'Star-forming galaxies', as in galaxies that are on or above the main sequence with $\log(\mathrm{SFR/SFR_{MS}(t)}) \geq -0.4$.
(ii) 'Intermediate galaxies', as in galaxies that are below the main sequence but with SFRs above that of a quiescent galaxy with $-1.3 < \log(\mathrm{SFR/SFR_{MS}(t)}) \leq -0.4$.
(iii) 'Quiescent galaxies' with $\log(\mathrm{SFR/SFR_{MS}(t)}) < -1.3$.

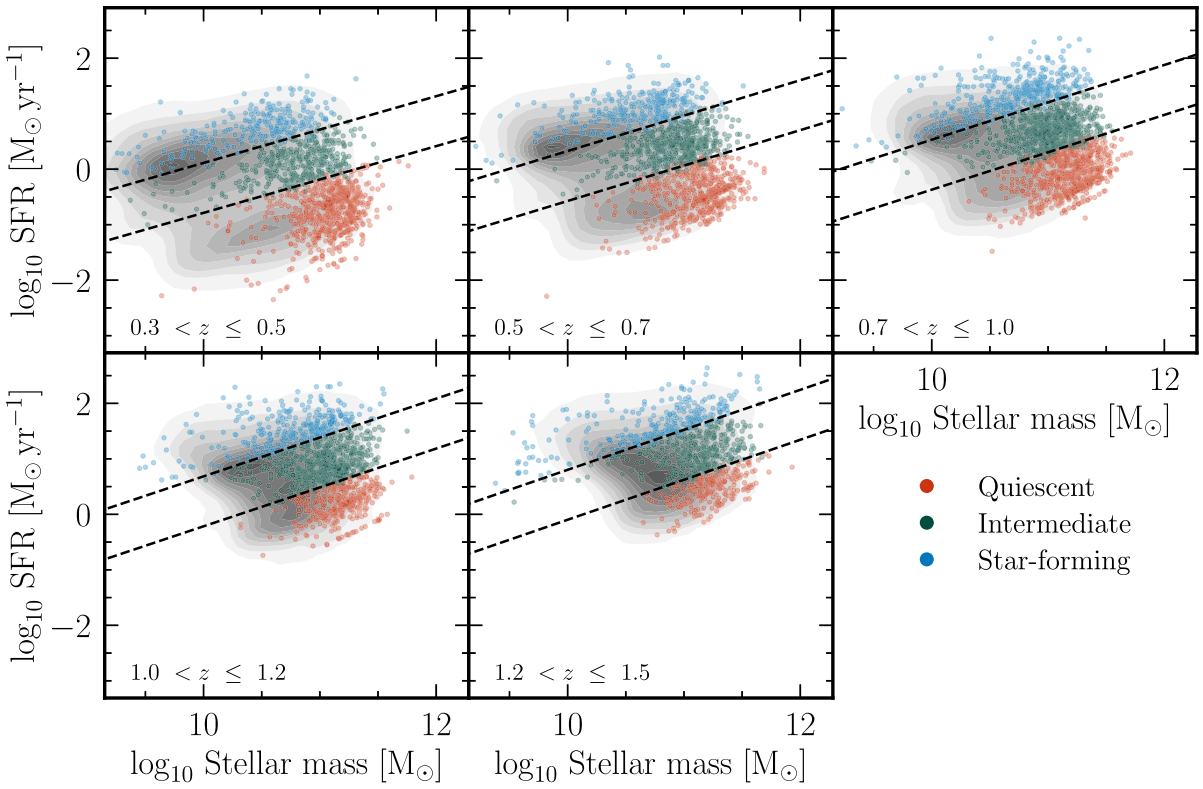

Figure 3. The location of LERGs on the SFR-M$_\star$ plane in five redshift bins across $0.3 < z \leq 1.5$. The LERG sample has been split into the subset that are hosted by quiescent (red), intermediate (green), and star-forming (blue) galaxies, defined based on the evolving main sequence (see Section 4). The diagonal dashed lines show the division lines used to select the three populations. The shaded contours show the distribution of the underlying MIR flux-selected parent sample along the SFR-M$_\star$ plane.

The typical scatter in the star-forming–main sequence relation derived by Speagle et al. (2014) is ∼0.2 dex. Following this, our selection of SFGs corresponds to sources within $\approx 2\sigma$ or above the main sequence, with quiescent galaxies defined as sources that are at least $\approx 6.5\sigma$ below the main sequence, and 'intermediate' galaxies lying in between these two populations. By defining our sample based on SFRs relative to the main sequence across different redshift bins, we account for the evolution of the galaxy population when comparing results across redshift bins as galaxies typically have higher SFRs at higher redshifts. Moreover, this analysis is also less affected by any systematic uncertainties on SFR estimates from photometry, although this is expected to be small (see Best et al. 2023).

In Fig. 3, we show the SFR–$M_\star$ distribution of the LERGs hosted by SFGs (blue), intermediate galaxies (green), and quiescent galaxies (red) across $0.3 < z \leq 1.5$ over five redshift bins, as in Fig. 1. The two diagonal dashed lines in each redshift bin denote the criteria used to separate the sources into the above three galaxy types relative to the main sequence. The grey shaded region in each redshift bin corresponds to the distribution of the mid-infrared flux-selected parent sample in the SFR–$M_\star$ plane (as described in Section 2.4) which was used for calculating the incidence of AGN in this section.

In Fig. 4, we compute the fraction of quiescent (left), intermediate (middle), and star-forming (right) galaxies that host a LERG with $L_{150\,\mathrm{MHz}} \geq 10^{24}\,\mathrm{W\,Hz^{-1}}$ as a function of stellar mass across $0.3 < z \leq 1.5$. The uncertainties are calculated following binomial statistics. In each panel, the black dashed line shows the local Universe relationship $f_{\mathrm{LERG}} = 0.01 \log_{10}(M_\star/10^{11}\,\mathrm{M}_\odot)^{2.5}$ for the LERGs (Janssen et al. 2012). The results shown in this figure extend beyond the analysis performed by Kondapally et al. (2022) of the binary separation of star-forming and quiescent galaxies.

Across the five redshift bins (shown by different coloured lines, as in Fig. 1), the LERGs hosted by quiescent galaxies (Q-LERGs hereafter) follow the same steep dependence on stellar mass with the same normalization out to $z \sim 1.5$; this is consistent with the observations of the overall LERG population in the local Universe, suggesting that LERGs within quiescent galaxies are also fuelled by the same mechanism, the cooling hot gas, right across cosmic time. As the star formation activity increases, going from intermediate to the star-forming populations in Fig. 4, the dependence on stellar mass flattens due to an increase in the incidence of LERGs within lower mass systems; as a result, the star-forming LERGs (SF-LERGs) are no longer consistent with the steep relation observed for the quiescent hosts, in particular at low masses. Moreover, as the fractions are calculated over the given galaxy type (rather than the entire galaxy population), the increase in the incidence of LERGs in SFGs at higher redshifts for fixed stellar mass indicates that SFGs are more likely to host a LERG at higher redshifts than in the local Universe. One potential cause for this result may be due to the increase in gas fractions at higher redshifts (e.g. Genzel et al. 2015; Tacconi et al. 2018); the more abundant gas supply that is available to fuel the more vigorous star formation within these host galaxies may also fuel the AGN.

Janssen et al. (2012) studied the dependence of LERG activity on galaxy colour at $z < 0.3$ using D4000 Å and u–r colours to separate sources into red, green, and blue galaxies. They found that

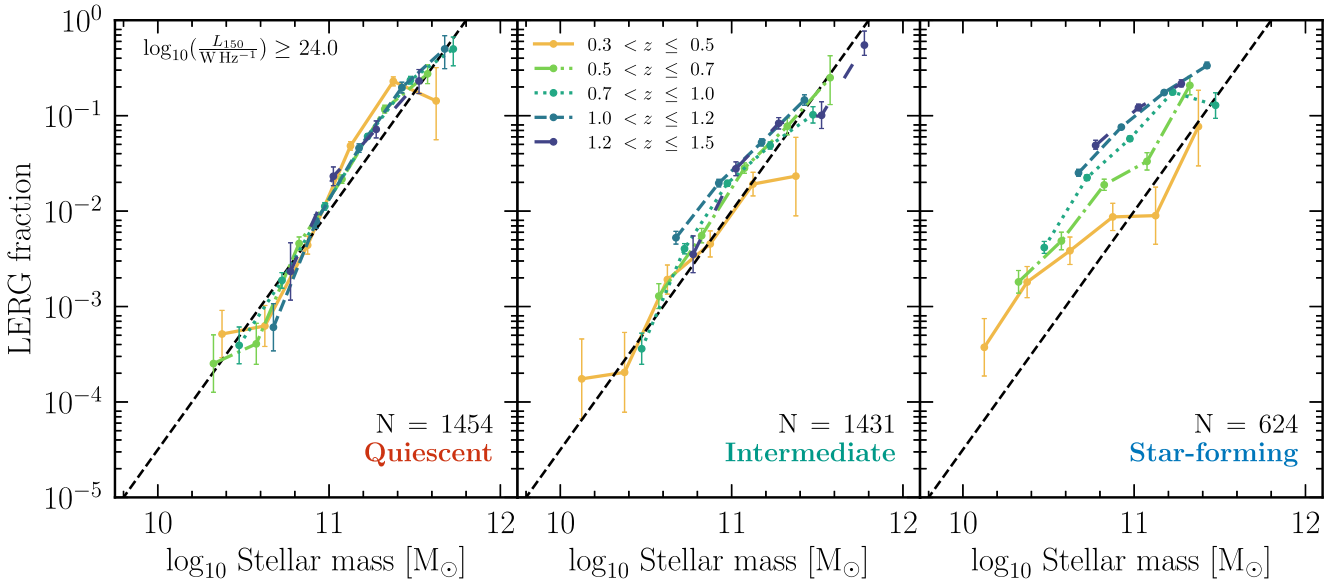

Figure 4. Fraction of quiescent (left), intermediate (middle), and star-forming (right) galaxies hosting a LERG with $L_{150\,\mathrm{MHz}} \geq 10^{24}\,\mathrm{W\,Hz^{-1}}$ as a function of their stellar mass across $0.3 < z \leq 1.5$. The host galaxy types for the LERGs are identified based on the offset from the evolving star-forming main sequence, with the number in each panel corresponding the number of LERGs hosted by each galaxy type across $0.3 < z \leq 1.5$ for the above radio luminosity limit. The LERGs hosted by quiescent galaxies show a steep dependence on stellar mass, that does not evolve with cosmic time; moving along the galaxy population, towards more star-forming systems, the incidence of LERGs increases at lower masses leading to a flattening of the relationship.

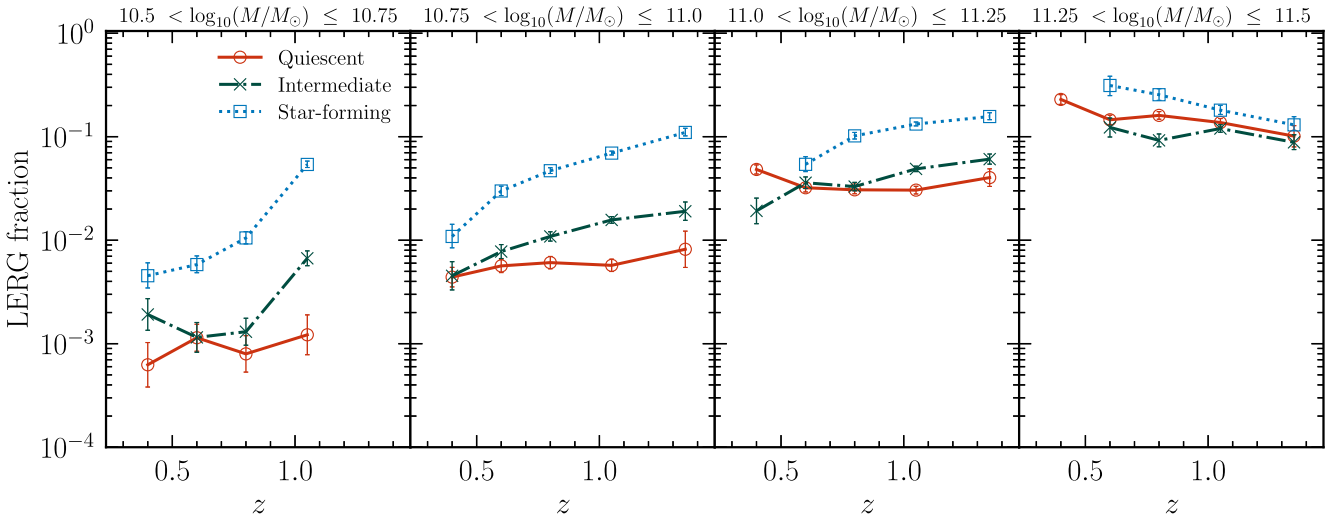

Figure 5. The incidence of LERGs with $L_{150\,\mathrm{MHz}} \geq 10^{24}\,\mathrm{W\,Hz^{-1}}$ across redshift, with panels showing increasing stellar mass bins from left to right. In each panel, the incidences of LERGs are calculated within different galaxy types: quiescent (red), intermediate (green), and star-forming (blue). Overall the incidence of LERGs increases with stellar mass across all galaxies, going from the left to the right panel. At low masses of $\log_{10}(M/\mathrm{M}_\odot) \leq 11$, galaxies with ongoing star formation activity (i.e. the intermediate and star-forming populations) are significantly more likely to host a LERG compared to quiescent galaxies, across all redshifts studied. At higher masses, the LERGs are found across the entire galaxy population, regardless of their star formation activity, at roughly the same rate.

compared to green or blue galaxies, red galaxies were more likely to host a LERG at high masses (by a factor of $\sim$ 2–3 times at $\log_{10}(M_\star/\mathrm{M}_\odot) \gtrsim 11$), with the incidence across galaxies of different colours becoming more similar at low masses. However, our results indicate that at high masses the incidence of LERGs across quiescent and SFGs becomes roughly similar. Some of the differences with Janssen et al. (2012) could be due to cosmic evolution; only $\sim$2 per cent of the LERGs identified by Janssen et al. (2012) were hosted by blue galaxies whereas LERGs are found to be more likely to be hosted by SFGs with increasing redshift (see Kondapally et al. 2022). We also note that while their separation of galaxies into red, green, and blue is analogous, it is not directly comparable to the quiescent, intermediate, and star-forming separation applied in this study.

Williams & Röttgering (2015) studied the incidence of radio-loud AGN on stellar mass out to $z \sim 2$ using early LOFAR observations. They found that the radio-loud AGN fraction (i.e. for LERGs and

HERGs combined) increased at low masses with increasing redshift, while staying roughly constant at high masses; this is in good agreement with our results. Compared to their results for the entire radio-loud population, we have shown that the flattening of the mass dependence at high redshifts is likely caused by an increased prevalence of LERGs hosted by SFGs. Recently, Wang et al. (2024) studied the incidence of radio-excess AGN in quiescent and SFGs out to higher redshifts. They find that radio-excess AGN are more likely to be found in massive quiescent galaxies compared to SFGs, which is broadly consistent with our results. Their analysis is carried out for a sample of all radio-excess AGN, which includes both the LERG and HERG populations, and is performed in bins of radio luminosity rather than integrated over all radio luminosities above a limit (as in this study); this prevents a more quantitative comparison with our results.

To better illustrate the stellar mass and any redshift dependence across different galaxy populations, in Fig. 5, we show the fraction of different galaxy types hosting a LERG (with $L_{150\,\mathrm{MHz}} \geq 10^{24}\,\mathrm{W\,Hz^{-1}}$) as a function of redshift within four stellar mass bins (separated by 0.25 dex) increasing in mass from left to right panels. In the lowest stellar mass bins with $10.5 < \log_{10}(M/\mathrm{M}_{\odot}) \leq 11$, there is a notable difference in the incidence of LERGs with increasing star formation activity. The fraction of LERGs hosted by quiescent galaxies is typically lower by an order of magnitude or more compared to the SFGs. The fraction of LERGs also increases with increasing redshift (by a factor of $\sim$ 2–8 out to $z \sim 1$) for intermediate and SFGs, whereas this remains largely flat for the quiescent galaxies. At $10.75 < \log_{10}(M/\mathrm{M}_{\odot}) \leq 11$, the SFGs are still more likely to host a LERG than quiescent galaxies at any redshift, with the LERG fraction increasing with increasing redshift for the more star-forming systems. The higher prevalence of LERG activity in SFGs compared to quiescent galaxies, coupled with the increase in the LERG fraction within SFGs with increasing redshift, results in the overall flattening of the relation seen for the SF-LERGs in Fig. 4. These results at low masses suggest that there is a causal link between the triggering of LERG activity and the cold gas fractions in SFGs, which increases at higher redshifts (e.g. Genzel et al. 2015; Tacconi et al. 2018). In the most massive bin, the incidence of LERGs remains largely consistent across different galaxy types: at $11.25 < \log_{10}(M/\mathrm{M}_{\odot}) \leq 11.5$, $\sim$ 10–20 per cent of all galaxies host a LERG, regardless of their star formation activity. This suggests that LERG activity in massive galaxies may be driven by the same mechanism across the galaxy population: cooling of hot gas from their haloes. Although the fraction of star-forming and quiescent galaxies hosting a LERG are similar at these high masses, there are more SFGs at higher redshifts than quiescent galaxies, so the bulk of the AGN activity in the early Universe occurs in galaxies that are not quiescent (see also Kondapally et al. 2022).

5 DISTRIBUTION OF THE EDDINGTON-SCALED ACCRETION RATES

Observations of different states of X-ray binaries (e.g. Remillard & McClintock 2006) and theoretical accretion disc models (e.g. Narayan & Yi 1994, 1995; Yuan & Narayan 2014) indicate a switch in the nature of the accretion flow occurring at Eddington-scaled accretion rates, λ_{Edd}, of around 1 per cent ($\lambda_{\mathrm{Edd}} = 0.01$), going from radiatively efficient accretion at higher accretion rates to radiatively inefficient (or advection dominated accretion) at lower accretion rates. In the local Universe, studies have previously found significant differences in the Eddington-scaled accretion rates of the LERGs and HERGs, with the LERGs typically accreting below 1 per cent of the Eddington rate, and the HERGs typically accreting at higher rates (e.g. Best & Heckman 2012; Mingo et al. 2014). These differences in the accretion rate properties have been used to explain many of the differences in the properties of the central AGN and their host galaxies between the LERGs and the HERGs (see reviews by Heckman & Best 2014; Tadhunter 2016; Hardcastle & Croston 2020; Magliocchetti 2022). More recent studies, which reach fainter radio luminosities, have found considerable overlap in the accretion rates between the two populations (e.g. Whittam et al. 2022). Here, we consider the accretion rates of the LERGs across the three different galaxy populations, and the HERGs.

The Eddington-scaled accretion rates can be estimated as

$$\lambda_{\mathrm{Edd}} = \frac{L_{\mathrm{rad}} + L_{\mathrm{mech}}}{L_{\mathrm{Edd}}}, \tag{2}$$

where L_{rad} is the bolometric radiative luminosity of the AGN, L_{mech} is the kinetic/mechanical luminosity from the radio jets, and L_{Edd} is the Eddington luminosity limit for each source. In the absence of emission line properties for the vast majority of the sources, the bolometric radiative luminosity is estimated from the best-fitting CIGALE SED model (see Best et al. 2023) for each source and is the sum of the AGN accretion disc luminosity and the AGN dust re-emitted luminosity, coming from the re-emitted infrared light due to dust surrounding the AGN. The mechanical luminosity of the jets can be estimated using the 1.4 GHz radio luminosity as $L_{\mathrm{kin,\,cav}} = 7 \times 10^{36} f_{\mathrm{cav}} \left(L_{1.4\,\mathrm{GHz}}/10^{25}\,\mathrm{W\,Hz^{-1}}\right)^{0.68}$ W (Cavagnolo et al. 2010; Heckman & Best 2014). We translate our observed 150 MHz radio luminosities to 1.4 GHz using a spectral index $\alpha = -0.7$. This scaling relation for the mechanical luminosity was determined by using the energy associated with expanding the radio lobes and inflating cavities in the hot X-ray gas observed in massive groups and clusters (e.g. Boehringer et al. 1993; Bîrzan et al. 2008; Cavagnolo et al. 2010; Timmerman et al. 2022). The Eddington limit for each AGN was then determined using $L_{\mathrm{Edd}} = 1.31 \times 10^{31} (M_{\mathrm{BH}}/\mathrm{M}_{\odot})\,\mathrm{W}$, where the black hole mass is estimated using the stellar mass as $M_{\mathrm{BH}} \approx 0.0014 M_{\star}$ (Häring & Rix 2004). Overall, the scaling relations used to estimate the mechanical luminosity and the black hole masses both have a considerable scatter of $\sim$0.7 and $\sim$0.3 dex, respectively.

While over 97 per cent of the HERGs have a measured AGN accretion disc and AGN dust luminosity, over 50 per cent of the LERGs hosted by intermediate and SFGs, and around 80 per cent of the LERGs hosted by quiescent galaxies have no AGN accretion disc or AGN dust luminosity assigned to them. This is in line with expectations as the LERGs are radiatively inefficient AGN and hence not expected to have significant infrared (radiative) luminosities. Sources with extremely low AGN fractions, $f_{\mathrm{AGN}} < 0.05$, are not assigned a radiative luminosity by CIGALE; such sources with no measured radiative luminosities, which are pre-dominantly LERGs, can bias our interpretations. To account for this, we derive an upper limit on the bolometric luminosity to be 5 per cent of the total dust luminosity (i.e. corresponding to an $f_{\mathrm{AGN}} = 0.05$) for sources with no measured bolometric luminosities (see below).

Using the above relation for the kinetic powers together with equation (2), the Eddington-scaled accretion rates were derived for the LERGs and HERGs within the sample, applying the same $L_{150\,\mathrm{MHz}} \geq 10^{24}\,\mathrm{W\,Hz^{-1}}$ limit to allow comparisons with the results in the rest of this paper. Fig. 6 shows the cumulative accretion rate distributions, where the top panel shows the Eddington-scaled ac-

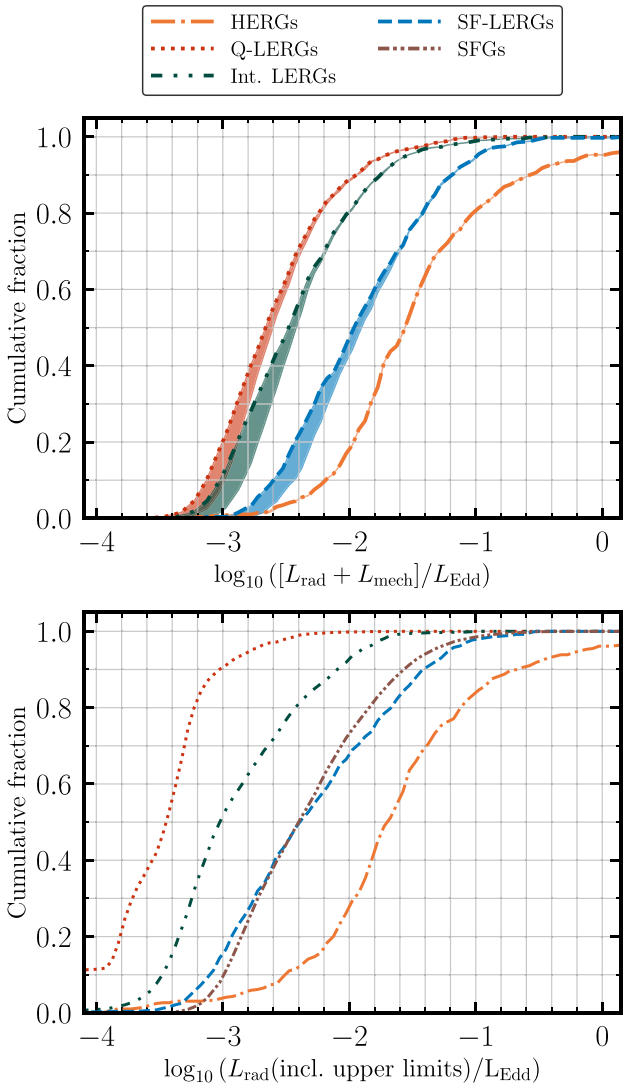

Figure 6. The cumulative distribution of the Eddington-scaled accretion rates for the LERGs within different galaxy populations, and for the HERGs. The top panel shows the Eddington-scaled accretion rates derived by combining the bolometric radiative AGN luminosity estimated from the SED fitting output and the mechanical jet luminosity. The thick, darker lines correspond to using $L_{\rm rad} = 0$ where there are no measurements, and the shaded region represents the effect of setting an upper limit on $L_{\rm rad}$ of 5 per cent of the total dust luminosity (see the text). The bottom panel shows the maximal accretion rates based on the radiative luminosity only, assigning the 5 per cent upper limit to the sources without measurement.

cretion rates determined by combining both the radiative bolometric luminosity and the mechanical luminosity, whereas the bottom panel shows those determined from the radiative bolometric luminosity alone. In the top panel of Fig. 6, the thick darker lines correspond to the accretion rates derived by setting $L_{\rm rad} = 0$ for sources with no measured value, while the shaded region indicates the effect of setting these at the 5 per cent upper limit instead, which shifts the distribution to higher values. The Eddington-scaled accretion rates are shown for the HERGs (orange) and the LERGs; the LERGs are further split into those hosted by quiescent (red), intermediate (green), and star-forming (blue) galaxies as previously defined in Section 4.

The HERGs typically have high-accretion rates, with $\gtrsim$80 per cent above $\lambda_{\rm Edd} \sim 0.01$; this is broadly consistent with HERGs being typically fuelled by radiatively efficient accretion. The quiescent LERGs typically have accretion rates below 1 per cent of the Eddington rate, which is consistent with fuelling occurring in a radiatively inefficient manner from cooling hot gas within their massive host galaxies. The intermediate LERGs show higher accretion rates while still being typically below 1 per cent of the Eddington rate. The SF-LERGs however have higher accretion rates which do not appear to be consistent with either the HERGs or the other subtypes of LERGs. The bottom panel of Fig. 6 shows the distribution considering the bolometric luminosities alone ($L_{\rm rad}/L_{\rm Edd}$), where the curve is derived using upper limits on $L_{\rm rad}$ where there is no measured value, as described above. Through a comparison with the top panel, we find that the radiative bolometric luminosities for the quiescent LERGs are significantly lower than the mechanical jet luminosities, with $L_{\rm rad}/L_{\rm Edd}$ typically below 0.1 per cent. In contrast, the bolometric radiative luminosities typically dominate over the mechanical jet luminosities for the HERGs. While ∼70 per cent of the SF-LERGs have $L_{\rm rad}/L_{\rm Edd} < 0.01$, the population occupies intermediate values of $L_{\rm rad}/L_{\rm Edd}$, between the Q-LERGs and HERGs. Based on observations in the local Universe (e.g. Best & Heckman 2012; Mingo et al. 2014), we do not expect a considerable population of LERGs to have accretion rates above 1 per cent of Eddington; we discuss the potential causes for this in Sections 5.1 and 5.2.

5.1 Potential source classification uncertainties

It is possible that source misclassification may have an impact on the observed accretion rate distributions seen in Fig. 6. In the presence of significant ongoing star formation, SED fitting routines may be less reliable in determining the presence of low-level AGN emission or robustly separating emission from AGN and star formation. This could lead to potential misclassification of sources, in particular between SF-LERGs and HERGs. However, it is important to note that the Best et al. (2023) classification scheme adopted mitigates this issue to an extent in various ways. First, instead of the best-fit $f_{\rm AGN}$, they used the 16th percentile of the $f_{\rm AGN}$ to identify the presence of radiative-mode AGN (for CIGALE, the criterion $f_{\rm AGN,16} > 0.06$ was used; > 0.1 in Boötes[3]) which is more robust to large uncertainties on the fitted AGN components due to the presence of star formation. Secondly, in addition to the above, Best et al. (2023) also compared the χ^2 values of BAGPIPES and MAGPHYS (which do not model AGN emission) with the values from AGNFITTER and CIGALE to identify radiative-mode AGN. Best et al. (2023) validated AGN identified via this classification method with mid-infrared colour–colour diagnostics, finding good agreement (see fig. 5 of Best et al. 2023).

We further validate the classification of sources using both recent spectroscopic observations and X-ray data for a subset of the sources, which is described in detail in Appendix B. First, we used observations from the Dark Energy Spectroscopic Instrument Early Data Release (DESI-EDR; DESI Collaboration 2023) to generate stacked optical spectra for each of Q-LERGs, SF-LERGs, HERGs, and SFGs, separately, as classified by Best et al. (2023). The

[3]A different threshold was used by Best et al. (2023) in Boötes as the $f_{\rm AGN}$ values derived from SED fitting were systematically higher, likely due to the differences in how the multiwavelength catalogue was constructed the Boötes field (see Best et al. 2023 for full details).

SF-LERG stack shows strong [O II] emission, indicative of star formation, and a lower [O III]/[O II] ratio than the HERGs showing that the SF-LERGs are dominated by 'normal' SFGs. However, the SF-LERG stack also shows slightly higher [O III] emission than the SFG stack indicating that there may be a small level of radiative-mode AGN contamination. Secondly, we used the *Chandra* Deep Wide-Field Survey (CDWFS; Masini et al. 2020) in the Boötes field to study the average X-ray properties of the different source classes. We find that the average (stacked) X-ray luminosities of each of Q-LERGs, intermediate LERGs, and SF-LERGs, show similar levels of X-ray emission, which are considerably lower than the HERGs. Our additional validation presented in Appendix B is focused on the average properties of each population rather than a source-by-source comparison, therefore, on average, we conclude that the LERGs hosted by intermediate and SFGs appear to be distinct to the HERGs, and show similar nuclear properties to the Q-LERGs. While there may be some potential misclassifications due to the nature of the limitations of the SED-fitting process, these results provide additional confidence that this does not have a significant impact on the robustness of the classifications used in this study.

5.2 Unreliable $L_{\rm bol}$ measurements for SF-LERGs

For sources with significant ongoing star formation, as in the case of the sources identified as SF-LERGs, it is possible that SED fitting routines may not be able to reliably model the contribution from AGN and star formation simultaneously, particularly for fainter galaxies with fewer robust photometric data points. To investigate this, we derive an equivalent $L_{\rm rad}/L_{\rm Edd}$ distribution for sources classified as SFGs[4] by Best et al. (2023) that also meet the star-forming criteria based on the the main sequence defined in Section 4; this is shown by the brown curve in Fig. 6 (bottom panel). We find that >60 per cent of the SFGs have no measured AGN fraction ($f_{\rm AGN}$; i.e. no measured 'radiative' luminosities). The remaining sources have very low $f_{\rm AGN}$ values (typically $\lesssim$0.05), but given the high total luminosities associated with ongoing star formation within the galaxies this still results in non-negligible $L_{\rm rad}$. Hence, the $L_{\rm rad}/L_{\rm Edd}$ distribution for the SFGs appears at intermediate values, and indeed is very similar to the SF-LERG distribution when incorporating the limits. In comparison, ∼90 per cent of the SF-LERGs have $f_{\rm AGN} \leq 0.05$, indicating low contribution from AGN emission. The similarities in the distributions of the two populations, where the key difference between how the two populations were selected is the presence of a radio-excess AGN for the SF-LERGs, highlights that the higher $L_{\rm rad}/L_{\rm Edd}$ observed for the SF-LERGs compared to Q-LERGs is primarily due to wrongly assigned luminosity from star formation processes rather than (missed) significant AGN emission arising from misclassified HERGs. Overall, this result suggests that the radiative luminosities estimated for the SF-LERGs through SED fitting processes may not be robust.

5.3 Comparison of Eddington-scaled accretion rates with literature

We now compare our results on the Eddington-scaled accretion rates of LERGs and HERGs shown in Fig. 6 with other studies in the literature. Following the above caveats regarding the robustness of the radiative luminosities estimated from SED fitting for the SF-LERGs, we do not attempt to overinterpret the Eddington-scaled accretion rates derived for this subgroup of LERGs in Fig. 6. Instead, here we primarily focus on comparing our Q-LERG and the HERG results to previous works, where we expect the derived radiative luminosities to be most robust.

Our results for the HERGs and the *quiescent* LERGs are in agreement with previous studies of the HERG and *overall* LERG populations in the local Universe (e.g. Best & Heckman 2012; Mingo et al. 2014). We find that there is more overlap between the LERG and HERG populations in our study, and while it is possible that this is a real effect, we suggest that these observations are also consistent with the combination of measurement uncertainties and selection effects. In particular, aside from the robustness of the radiative luminosities for SF-LERGs discussed above, our use of a scaling relationship to estimate black hole masses has considerable scatter, compared to the more robust measurements by Best & Heckman (2012) using spectra. Such scatter in the empirical scaling relationship can spread out the intrinsic Eddington-rate distributions of the two populations resulting in more apparent overlap; prospects for overcoming these limitations are discussed in Sections 6 and 7. Moreover, as we showed in Fig. 5 (and in Kondapally et al. 2022), SF-LERGs are expected to be less common at low redshifts studied by Best & Heckman (2012). Additionally, the use of emission line diagnostics to select LERGs by Best & Heckman (2012), which requires low line fluxes or equivalent widths from the [O II] and [O III] lines may select against star-forming hosts of LERGs.

Recently, Whittam et al. (2022) used the MeerKAT International GHz Tiered Extragalactic Exploration (MIGHTEE) early-science observations of the COSMOS field at 1.4 GHz to study the properties of LERGs and HERGs. Their data covers an area of $\sim 1\,{\rm deg}^2$ and reaches a noise level of $\sim$4 μJy beam^{-1}, comparable in-depth to our LoTSS Deep Fields data assuming a standard spectral index. Whittam et al. (2022) found considerable overlap in the Eddington-scaled accretion rates between their LERGs and HERGs. Overall, Whittam et al. (2022) have suggested that at higher redshifts and lower radio luminosities, the distinction between the LERG and HERG populations becomes less clear, with their host galaxy properties also becoming more similar. However, Whittam et al. (2022) also use the same scaling relationships to determine the jet mechanical luminosity and the black hole masses as our study, which as discussed above leads to a spread in the derived Eddington-scaled accretion rate distributions, and hence more overlap in the LERG and HERG populations. It is worth noting that the classification of LERGs at higher redshifts by Whittam et al. (2022) are less robust, in particular due to the X-ray data which limits their X-ray AGN classification to $z < 0.5$. As a result, they are only able to classify sources as 'LERGs' at $z < 0.5$, and instead identify a sample of 'probable LERGs' at higher redshifts. The Eddington-rate distribution for their 'probable LERG' sample extends to higher values than their LERG sample; it is therefore possible that their 'probable LERGs' could be contaminated by misclassified HERGs, and could suffer the same potential biases as our SF-LERGs whereby their radiative luminosities, and hence accretion rates, may be overestimated due to the presence of strong star formation. If this is not the case, then this would imply that the SF-LERGs indeed have higher bolometric luminosities, which would have interesting implications for the nature of these sources. We also note that the sample used by Whittam et al. (2022) probes higher redshifts than our

[4]Here, SFGs are defined as sources that do not display signs of either radio-excess AGN or radiative-mode AGN.

sample, which may also impact the detailed comparison with their study.

6 ON THE FUELLING OF LERGS AND HERGS ACROSS THE GALAXY POPULATION

The dependence of AGN activity on stellar mass and SFR presented in Sections 3 and 4 can be combined with the accretion rate properties derived in Section 5 to understand the nature of the faint LERG and HERG populations in the early Universe as traced by our observations. Our results from Figs 4 and 5 suggest that LERGs may be fuelled by multiple processes based on the available fuel supply and the stellar mass. Fuelling from hot gas is more likely to occur in massive galaxies, which also host massive black holes, and such fuelling typically occurs at low accretion rates and leads to the formation of a LERG. Our observations of LERGs across the galaxy population support a scenario where this process likely fuels the AGN in massive galaxies regardless of their star formation activity, effectively setting a 'minimum' level of LERG activity. This naturally explains the existence of the quiescent LERGs, which have low accretion rates (as seen in Fig. 6) that can be associated with fuelling from hot gas, and which are found in massive galaxies, resulting in the steep stellar mass relation observed in Fig. 4. In massive galaxies with higher SFRs, the same process may also fuel the AGN; this is supported by our results in Fig. 5 which show that at high masses, all galaxies, regardless of galaxy type, have roughly the same level of LERG activity (or a marginally higher level in SF-LERGs), pointing to a common fuelling process from hot gas. We note that the similarities in the incidence of LERGs in massive galaxies, which have massive dark matter haloes, may also suggest that the environment is an important factor in accretion from hot gas (see e.g. Tasse et al. 2008; Sabater et al. 2013; Mingo et al. 2019; Hardcastle & Croston 2020); a detailed modelling of the environments of these AGN is outside the scope of this paper.

In galaxies with high levels of star formation activity, there is an abundant supply of cold gas which can fuel both star formation and black hole growth. Therefore, we suggest that there may be an additional fuelling mechanism associated with the cold gas that fuels LERGs in galaxies with higher star formation activity; this is particularly important in lower mass galaxies. In this scenario, we would expect a higher level of LERG activity in galaxies with higher star formation activity at a fixed stellar mass; we observe a factor of 2–10 higher LERG incidence in SFGs compared to quiescent galaxies, as seen in Fig. 5. Additionally, in both Figs 4 and 5, we see that for a given stellar mass, the incidence of LERGs in SFGs increases with increasing redshift, when the gas fractions were also higher. Moreover, Heckman et al. (2024) find that the evolution of the cosmic energy budget from AGN jets is well correlated with the quenching rate, suggesting that the SF-LERGs may be connected to the quenching of SFGs. We note that although the presence of abundant cold gas is capable of fuelling the AGN at high rates, this does not necessarily mean that this always occurs (see Hardcastle 2018); therefore, if LERGs are defined as AGN fuelling below 1 per cent of the Eddington-rate, then it is possible for cold gas to supply this. We note that the stochastic nature of accretion can be coupled to the different time-scales involved in the generation of the radio jets and accretion disc structure, which can complicate the interpretations.

The picture for the HERGs appears more straightforward, with HERGs typically being found in star-forming systems, where they are fuelled at high accretion rates in a radiatively efficient manner by the cold gas present within their star-forming host galaxies, broadly consistent with previous studies at lower redshift (e.g. Best & Heckman 2012; Mingo et al. 2014). It is not clear how the population of HERGs accreting at low rates fit into this picture, however we note that the large scatter in the black hole mass–stellar mass relationship, and in the radio luminosity–jet kinetic power relationship may broaden the observed accretion rate distribution.

7 CONCLUSIONS

In this paper, we have used data from the LOFAR Deep Fields to study the host galaxy properties of radio-AGN out to $z = 1.5$. The three fields studied, ELAIS-N1, Lockman Hole, and Boötes, all benefit from having deep wide-area coverage from the UV to far-infrared wavelengths over $\sim 25\,\mathrm{deg}^2$. This data set was used to measure robust physical galaxy properties and for the identification of a sample of radio-AGN, which we further split into LERGs and HERGs. The host galaxy properties of these AGN were compared to a mid-infrared selected parent sample of the underlying galaxy population. Using this, we have presented robust measurements of the incidence of radio-AGN activity on stellar mass, SFR, and black hole accretion rate across $0.3 < z \leq 1.5$. We divided the AGN population based on their star formation activity relative to the main sequence of star formation into three groups: quiescent, intermediate, and star-forming hosts. In our analysis, we compute the Eddington-scaled accretion rates, λ_{Edd} for the AGN, by combining the bolometric radiative luminosity and mechanical luminosity from the jets. Our main conclusions are as follows:

(i) The LERGs show a steep dependence on stellar mass with some evidence of flattening at higher redshifts, as found by previous studies. The HERGs show a similarly steep relation, but with significantly lower prevalence than the LERGs at all stellar masses.

(ii) HERGs are pre-dominantly found in galaxies with ongoing star formation activity, across redshift, suggesting the need for cold gas supply to trigger HERG activity. In contrast, we find that LERG activity occurs across the galaxy population, in both quiescent and SFGs, with LERGs pre-dominantly hosted by SFGs in the early Universe.

(iii) The HERGs typically accrete above 1 per cent of the Eddington-scaled accretion rates, which is broadly consistent with previous studies in the local Universe.

(iv) When split into different galaxy groups based on star formation activity, the quiescent LERGs show typical accretion rates below 1 per cent of the Eddington-rate; this is consistent with results for the *overall* LERG population in the local Universe. We find that the radiative luminosities (and hence accretion rates) derived for SF-LERGs from SED fitting are likely not robust; this highlights the need for spectroscopic data to robustly characterize AGN accretion properties.

(v) The incidence of LERGs in quiescent galaxies has a steep dependence on stellar mass which does not vary with redshift; this is found to be consistent with fuelling occurring at low Eddington rates from hot gas.

(vi) LERG activity depends on both stellar mass and SFR, suggesting a different fuelling mechanism of LERGs across the galaxy population. We find that at high masses, LERGs are roughly equally as likely to be found in quiescent or SFGs: at high masses, ∼10–20 per cent of the galaxies host a LERG irrespective of the star formation activity.

(vii) At lower masses, LERG activity is significantly more likely to be hosted in galaxies with higher star formation activity, by a factor of up to 10 compared to quiescent galaxies. This suggests

that at lower masses, in particular within SFGs, there may be an additional mechanism that triggers LERG activity.

In summary, our recent work has found a significant population of LERGs hosted by SFGs, in contrast to expectations from studies in the local Universe. Our observations suggest that accretion from the hot gas provides a minimum level of incidence for the LERGs with an additional fuelling mechanism from cold gas providing an enhancement. In massive galaxies where the incidence is high, hot gas accretion dominates the fuelling across the galaxy population, regardless of star formation activity. However in low-mass galaxies, fuelling from cold gas provides an enhancement of LERG activity within SFGs in particular. The precise fuelling mechanisms that trigger LERG activity in SFGs remain unclear at present, although our results suggest that this may be occurring from cold gas. Further evidence in support of this scenario comes from the incidence of LERGs increasing with both increasing star formation activity and at higher redshifts, when the gas fractions were also higher.

Going beyond the global galaxy properties towards a characterization of their molecular gas properties, in comparison to a matched sample of LERGs and HERGs in different galaxy types, will be necessary to understand the fuelling processes at play. Our results also find some overlap in the Eddington-scaled accretion rates of LERGs and HERGs; it is possible that some of this observed overlap could be associated with the stochastic nature of accretion, scatter in the empirical scaling relations, or potential uncertainties in source classifications and derived radiative luminosities. To overcome remaining uncertainties in source classification and in estimating galaxy and AGN properties requires the availability of spectra; emission line diagnostics allows the most robust method of identifying radiatively efficient versus inefficient activity (e.g. Best & Heckman 2012; Whittam et al. 2018). A similar analysis has recently been applied to the wide-area LoTSS DR2 data set (Hardcastle et al. 2023; Drake et al. 2024) using Sloan Digital Sky Survey (SDSS) spectroscopic observations; however current spectroscopic data sets are only able to cover a small fraction of the LOFAR-detected sources. The upcoming WEAVE–LOFAR survey (Smith et al. 2016), using the new William Herschel Telescope Enhanced Area Velocity Explorer (WEAVE) instrument (Jin et al. 2024) onboard the William Herschel Telescope, will provide dedicated follow-up optical spectra for a large number of LOFAR-detected sources. This will enable robust source classification and identification of different AGN types, and the characterization of their properties including radiative luminosities and black hole masses.

ACKNOWLEDGEMENTS

This paper is based (in part) on data obtained with the International LOFAR Telescope (ILT) under project codes LC0_015, LC2_024, LC2_038, LC3_008, LC4_008, LC4_034, and LT10_01. LOFAR (van Haarlem et al. 2013) is the Low-Frequency Array designed and constructed by ASTRON. It has observing, data processing, and data storage facilities in several countries, which are owned by various parties (each with their own funding sources), and which are collectively operated by the ILT foundation under a joint scientific policy. The ILT resources have benefitted from the following recent major funding sources: CNRS-INSU, Observatoire de Paris and Université d'Orléans, France; BMBF, MIWF-NRW, MPG, Germany; Science Foundation Ireland (SFI), Department of Business, Enterprise and Innovation (DBEI), Ireland; NWO, the Netherlands; The Science and Technology Facilities Council, UK; and Ministry of Science and Higher Education, Poland. For the purpose of open access, the authors have applied a Creative Commons Attribution (CC BY) licence to any Author Accepted Manuscript version arising from this submission. This research made use of ASTROPY, a community-developed core PYTHON package for astronomy (Astropy Collaboration 2013, 2018) hosted at http://www.astropy.org/, and of MATPLOTLIB (Hunter 2007).

RK and PNB acknowledge support from the UK Science and Technologies Facilities Council (STFC) via grant ST/V000594/1. MIA acknowledges support from the UK STFC studentship under the grant ST/V506709/1. KM has been supported by the Polish National Science Centre (UMO-2018/30/E/ST9/00082). BM acknowledges support from the UK STFC under grant ST/T000295/1. BM further acknowledges support from UK Research and Innovation STFC for an Ernest Rutherford Fellowship (grant number ST/Z510257/1). SD acknowledges support from a STFC studentship via grant ST/W507490/1. IP acknowledges support from INAF under the Large Grant 2022 funding scheme (project 'MeerKAT and LOFAR Team up: a Unique Radio Window on Galaxy/AGN co-Evolution'). DJBS acknowledges support from the UK STFC under grants ST/V000624/1 and ST/Y001028/1. We thank Dr. James Aird for helpful discussions on the X-ray stacking analysis. For the purpose of open access, the author has applied a Creative Commons Attribution (CC BY) licence to any Author Accepted Manuscript version arising from this submission.

DATA AVAILABILITY

The data set used in this study comes primarily from the LoTSS Deep Fields Data Release 1. The corresponding radio data are presented by Sabater et al. (2021) and Tasse et al. (2021), the multiwavelength data, host galaxy counterparts, and photometric redshifts are presented by Duncan et al. (2021) and Kondapally et al. (2021), with the source classifications presented by Best et al. (2023). The images and catalogues are publicly available at https://lofar-surveys.org/deepfields.html. The SED fitting output for the mid-infrared parent sample is presented by Smith et al. (2021).

REFERENCES

Aird J., Coil A. L., Georgakakis A., 2017, MNRAS, 465, 3390
Allen S. W., Dunn R. J. H., Fabian A. C., Taylor G. B., Reynolds C. S., 2006, MNRAS, 372, 21
Arnaudova M. I. et al., 2024, MNRAS, 528, 4547
Astropy Collaboration, 2013, A&A, 558, A33
Astropy Collaboration, 2018, AJ, 156, 123
Best P. N., Heckman T. M., 2012, MNRAS, 421, 1569
Best P. N., Kauffmann G., Heckman T. M., Brinchmann J., Charlot S., Ivezić Ž., White S. D. M., 2005a, MNRAS, 362, 25
Best P. N., Kauffmann G., Heckman T. M., Ivezić Ž., 2005b, MNRAS, 362, 9
Best P. N., Kaiser C. R., Heckman T. M., Kauffmann G., 2006, MNRAS, 368, L67
Best P. N., von der Linden A., Kauffmann G., Heckman T. M., Kaiser C. R., 2007, MNRAS, 379, 894
Best P. N., Ker L. M., Simpson C., Rigby E. E., Sabater J., 2014, MNRAS, 445, 955
Best P. N. et al., 2023, MNRAS, 523, 1729
Bîrzan L., McNamara B. R., Nulsen P. E. J., Carilli C. L., Wise M. W., 2008, ApJ, 686, 859
Boehringer H., Voges W., Fabian A. C., Edge A. C., Neumann D. M., 1993, MNRAS, 264, L25
Boller T., Freyberg M. J., Trümper J., Haberl F., Voges W., Nandra K., 2016, A&A, 588, A103

Boquien M., Burgarella D., Roehlly Y., Buat V., Ciesla L., Corre D., Inoue A. K., Salas H., 2019, A&A, 622, A103
Bower R. G., Benson A. J., Malbon R., Helly J. C., Frenk C. S., Baugh C. M., Cole S., Lacey C. G., 2006, MNRAS, 370, 645
Brown M. J. I., Dey A., Jannuzi B. T., Brand K., Benson A. J., Brodwin M., Croton D. J., Eisenhardt P. R., 2007, ApJ, 654, 858
Brown M. J. I. et al., 2008, ApJ, 682, 937
Burgarella D., Buat V., Iglesias-Páramo J., 2005, MNRAS, 360, 1413
Butler A., Huynh M., Kapińska A., Delvecchio I., Smolčić V., Chiappetti L., Koulouridis E., Pierre M., 2019, A&A, 625, A111
Calistro Rivera G., Lusso E., Hennawi J. F., Hogg D. W., 2016, ApJ, 833, 98
Carnall A. C., McLure R. J., Dunlop J. S., Davé R., 2018, MNRAS, 480, 4379
Cattaneo A. et al., 2009, Nature, 460, 213
Cavagnolo K. W., McNamara B. R., Nulsen P. E. J., Carilli C. L., Jones C., Bîrzan L., 2010, ApJ, 720, 1066
Ching J. H. Y. et al., 2017, MNRAS, 464, 1306
Cochrane R. K. et al., 2023, MNRAS, 523, 6082
Croston J. H. et al., 2019, A&A, 622, A10
Croton D. J. et al., 2006, MNRAS, 365, 11
da Cunha E., Charlot S., Elbaz D., 2008, MNRAS, 388, 1595
Das S. et al., 2024, MNRAS, 531, 977
de Ruiter H. R., Willis A. G., Arp H. C., 1977, A&AS, 28, 211
Delvecchio I. et al., 2017, A&A, 602, A3
Delvecchio I. et al., 2022, A&A, 668, A81
DESI Collaboration 2024, AJ, 168, 58
Drake A. B. et al., 2024, MNRAS, 534, 1107
Duncan K. J. et al., 2018a, MNRAS, 473, 2655
Duncan K. J., Jarvis M. J., Brown M. J. I., Röttgering H. J. A., 2018b, MNRAS, 477, 5177
Duncan K. J. et al., 2021, A&A, 648, A4
Dunlop J. S., Peacock J. A., 1990, MNRAS, 247, 19
Fabian A. C., 2012, ARA&A, 50, 455
Ferrarese L., Merritt D., 2000, ApJ, 539, L9
Fitzpatrick E. L., 1999, PASP, 111, 63
Gendre M. A., Best P. N., Wall J. V., Ker L. M., 2013, MNRAS, 430, 3086
Genzel R. et al., 2015, ApJ, 800, 20
Gürkan G. et al., 2018, MNRAS, 475, 3010
Hardcastle M. J., 2009, in Saikia D. J., Green D. A., Gupta Y., Venturi T., eds, ASP Conf. Ser., Vol. 407, The Low-Frequency Radio Universe. Astron. Soc. Pac., San Francisco, p. 121
Hardcastle M., 2018, Nat. Astron., 2, 273
Hardcastle M. J., Croston J. H., 2020, New A Rev., 88, 101539
Hardcastle M. J., Evans D. A., Croston J. H., 2007, MNRAS, 376, 1849
Hardcastle M. J. et al., 2023, A&A, 678, A151
Häring N., Rix H.-W., 2004, ApJ, 604, L89
Heckman T. M., Best P. N., 2014, ARA&A, 52, 589
Heckman T., Roy N., Best P., Kondapally R., 2024, preprint (arXiv:2410.09157)
Hunter J. D., 2007, Comput. Sci. Eng., 9, 90
Igo Z. et al., 2024, A&A, 686, A43
Janssen R. M. J., Röttgering H. J. A., Best P. N., Brinchmann J., 2012, A&A, 541, A62
Jin S. et al., 2024, MNRAS, 530, 2688
Kennicutt R. C. J., 1998, ARA&A, 36, 189
Kenter A. et al., 2005, ApJS, 161, 9
Kondapally R. et al., 2021, A&A, 648, A3
Kondapally R. et al., 2022, MNRAS, 513, 3742
Kondapally R. et al., 2023, MNRAS, 523, 5292
Kormendy J., Ho L. C., 2013, ARA&A, 51, 511
Lehmer B. D., Alexander D. M., Bauer F. E., Brandt W. N., Goulding A. D., Jenkins L. P., Ptak A., Roberts T. P., 2010, ApJ, 724, 559
Lehmer B. D. et al., 2016, ApJ, 825, 7
Leja J., Johnson B. D., Conroy C., van Dokkum P. G., Byler N., 2017, ApJ, 837, 170
Magliocchetti M., 2022, A&A Rev., 30, 6
Masini A. et al., 2020, ApJS, 251, 2
McNamara B. R., Nulsen P. E. J., 2007, ARA&A, 45, 117
Merritt D., Ferrarese L., 2001, MNRAS, 320, L30
Mineo S., Gilfanov M., Lehmer B. D., Morrison G. E., Sunyaev R., 2014, MNRAS, 437, 1698
Mingo B., Hardcastle M. J., Croston J. H., Dicken D., Evans D. A., Morganti R., Tadhunter C., 2014, MNRAS, 440, 269
Mingo B. et al., 2019, MNRAS, 488, 2701
Mohan N., Rafferty D., 2015, Astrophysics Source Code Library, record ascl:1502.007
Narayan R., Yi I., 1994, ApJ, 428, L13
Narayan R., Yi I., 1995, ApJ, 452, 710
Noll S., Burgarella D., Giovannoli E., Buat V., Marcillac D., Muñoz-Mateos J. C., 2009, A&A, 507, 1793
Pracy M. B. et al., 2016, MNRAS, 460, 2
Remillard R. A., McClintock J. E., 2006, ARA&A, 44, 49
Sabater J., Best P. N., Argudo-Fernández M., 2013, MNRAS, 430, 638
Sabater J. et al., 2019, A&A, 622, A17
Sabater J. et al., 2021, A&A, 648, A2
Schlegel D. J., Finkbeiner D. P., Davis M., 1998, ApJ, 500, 525
Shakura N. I., Sunyaev R. A., 1973, A&A, 24, 337
Simpson C., Westoby P., Arumugam V., Ivison R., Hartley W., Almaini O., 2013, MNRAS, 433, 2647
Smith D. J. B. et al., 2016, in Reylé C., Richard J., Cambrésy L., Deleuil M., Pécontal E., Tresse L., Vauglin I., eds, SF2A-2016: Proceedings of the Annual meeting of the French Society of Astronomy and Astrophysics. p. 271
Smith D. J. B. et al., 2021, A&A, 648, A6
Smolčić V. et al., 2009, ApJ, 696, 24
Smolčić V. et al., 2017a, A&A, 602, A2
Smolčić V. et al., 2017b, A&A, 602, A6
Somerville R. S., Davé R., 2015, ARA&A, 53, 51
Speagle J. S., Steinhardt C. L., Capak P. L., Silverman J. D., 2014, ApJS, 214, 15
Sutherland W., Saunders W., 1992, MNRAS, 259, 413
Tacconi L. J. et al., 2018, ApJ, 853, 179
Tadhunter C., 2016, A&A Rev., 24, 10
Tasse C., Best P. N., Röttgering H., Le Borgne D., 2008, A&A, 490, 893
Tasse C. et al., 2021, A&A, 648, A1
Timmerman R., van Weeren R. J., Botteon A., Röttgering H. J. A., McNamara B. R., Sweijen F., Bîrzan L., Morabito L. K., 2022, A&A, 668, A65
van Haarlem M. P. et al., 2013, A&A, 556, A2
Wang Y. et al., 2024, A&A, 685, A79
Whittam I. H., Prescott M., McAlpine K., Jarvis M. J., Heywood I., 2018, MNRAS, 480, 358
Whittam I. H. et al., 2022, MNRAS, 516, 245
Williams W. L., Röttgering H. J. A., 2015, MNRAS, 450, 1538
Williams W. L. et al., 2018, MNRAS, 475, 3429
Williams W. L. et al., 2019, A&A, 622, A2
Yuan F., Narayan R., 2014, ARA&A, 52, 529

APPENDIX A: RADIO-EXCESS SELECTION COMPLETENESS CORRECTIONS

The selection of AGN using the radio-excess based on the radio-luminosity–SFR relation may lead to misclassification of low (radio) luminosity AGN as SFGs. Consider that the 150 MHz radio luminosity for each source is the sum of the radio luminosity arising from the AGN (jets) and from star formation processes as follows, $L_{150\,\mathrm{MHz}} = L_{\mathrm{AGN}} + L_{\mathrm{SF}}$. Therefore, applying a $L_{150\,\mathrm{MHz}}$ limit, as done throughout most of the analysis in this paper, will not uniformly select AGN above the same luminosity limit in all galaxies. Specifically, for a given AGN luminosity, sources hosted in more SFGs will be less likely to satisfy the radio-excess criterion, compared to quiescent host galaxies. This introduces an incompleteness in the radio-excess AGN selection at high SFRs. This is particularly relevant for our analysis, where we apply a 150 MHz

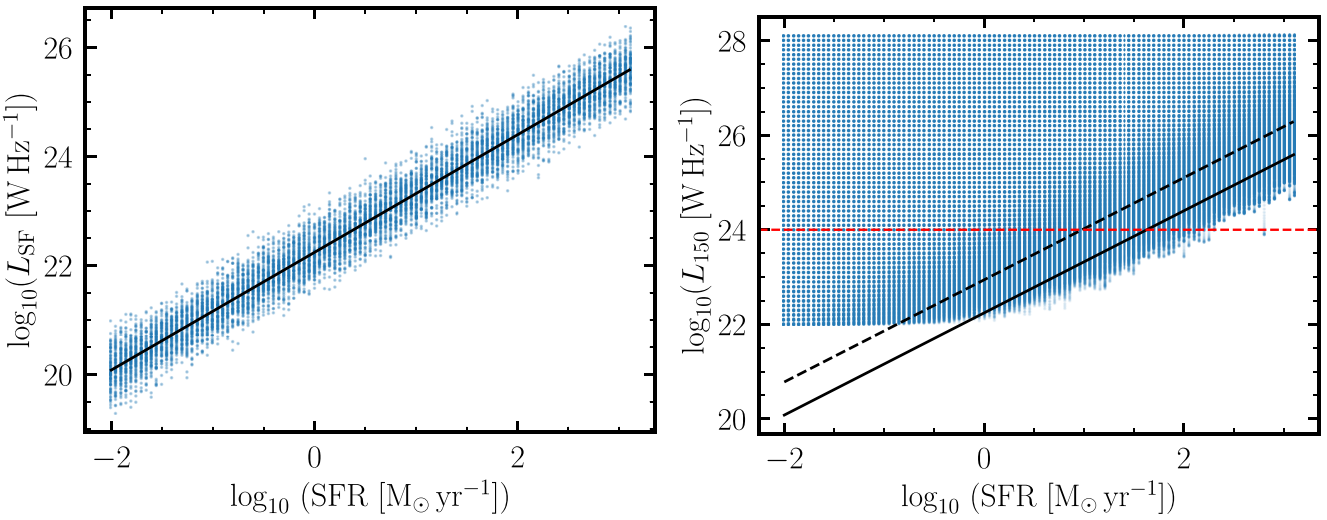

Figure A1. Results of the Monte Carlo simulation to quantify the completeness of the radio-excess AGN selection. *Left:* the simulated relationship between the 150 MHz radio-luminosity and SFR for SFGs, with a simulated Gaussian scatter of 0.3 dex. *Right:* the total 150 MHz radio luminosity for simulated sources, calculated as the sum of the $L_{\rm AGN}$ and $L_{\rm SF}$ components (from the left panel), as a function of the SFR (see the text). The black solid line in both panels shows the radio luminosity–SFR relation of Best et al. (2023). The dashed black line shows the radio-excess criterion (0.7 dex above the relation) used to identify radio-excess AGN. The red horizontal line corresponds to the radio luminosity limit of $L_{150\,\rm MHz} \geq 10^{24}$ W Hz^{-1} applied for the analysis.

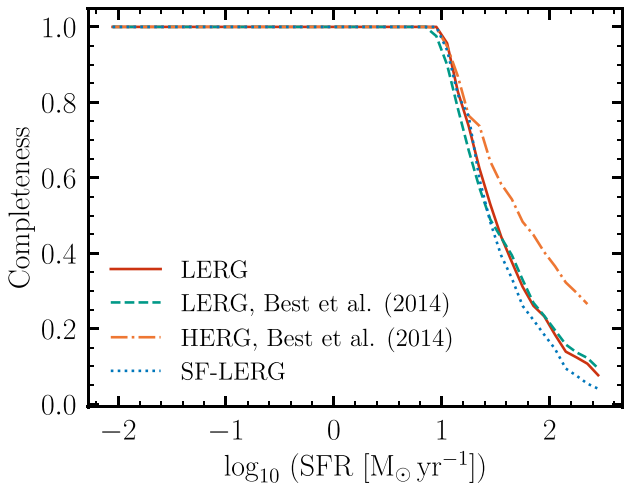

Figure A2. Radio-excess AGN selection completeness as a function of SFR for LERGs, SF-LERGs, and HERGs. The completeness curves are derived by convolving the Monte Carlo simulation with the radio luminosity function (see the text). Therefore, in each case, the curves correspond to the completeness in the radio-excess selection for the specific AGN type above a limiting luminosity of $L_{150\,\rm MHz} \geq 10^{24}$ W Hz^{-1}.

radio luminosity limit ($L_{150\,\rm MHz} \geq 10^{24}$ W Hz^{-1}) to account for the radio flux density incompleteness effects out to $z \sim 1.5$ (see Section 3). Choosing a sufficiently high radio luminosity limit would ensure a largely complete sample of luminous AGN, however would limit the analysis to the most luminous sources and results in poorer statistics.

An alternative approach is to assess the impact of the above selection effect on the results derived in this paper, which is described here. We first generated mock sources by simulating their radio luminosities, which are assumed to be described by a two-component model, $L_{150\,\rm MHz} = L_{\rm AGN} + L_{\rm SF}$, where $L_{\rm AGN}$ is the AGN component, and $L_{\rm SF}$ is the star formation component to the radio luminosity. There is a tight correlation between the radio luminosity and SFR of SFGs (e.g. Gürkan et al. 2018; Smith et al. 2021). The $L_{\rm SF}$ component was modelled as a Gaussian centred on the radio luminosity–SFR relation derived for the LoTSS-Deep sample by Best et al. (2023) and used for the radio-excess selection, $\log_{10}(L_{\rm SF,mean}/{\rm W\,Hz^{-1}}) = 22.24 + 1.08\log_{10}({\rm SFR}/{\rm M_\odot\,yr^{-1}})$, with a standard deviation of 0.3 dex (following the typical scatter in the relationship; see Smith et al. 2021 and Cochrane et al. 2023). SFRs spanning 5 orders of magnitude, between $-2 < \log_{10}({\rm SFR}/{\rm M_\odot\,yr^{-1}}) < 3$ were used to calculate $L_{\rm SF}$, generating a distribution of 10 000 simulated sources along the $L_{\rm SF}$ − SFR plane. For visualization purposes, we show the resulting distribution for a fraction of the sources in Fig. A1. The $L_{\rm AGN}$ component was finely sampled in 100 bins from a uniform distribution spanning $L_{150\,\rm MHz} = 10^{23} - 10^{28}$ W Hz^{-1}, covering the full range of luminosities probed by the AGN sample used in this analysis (see Kondapally et al. 2022; Best et al. 2023).

For each $L_{\rm AGN}$ value, the total 150 MHz radio luminosity, $L_{150\,\rm MHz}$, was calculated by summing the two components together, to transform the above into a distribution of 10 000 sources along the $L_{150\,\rm MHz}$ − SFR plane. This process is repeated for each $L_{\rm AGN}$ to capture the effect of varying the AGN luminosity on the total 150 MHz luminosity along this plane by generating a sample of 100 × 10 000 sources. For visualization purposes again, we show this distribution for a fraction of the simulated sources in the right panel of Fig. A1. As the completeness depends on both radio luminosity and SFR, we split this large sample into narrow bins in $L_{150\,\rm MHz}$ and SFR, and for each bin, we calculated the fraction of simulated sources (weighted by the radio luminosity function; see below) that would satisfy the radio-excess selection, as in, with $L_{150\,\rm MHz}$ above 0.7 dex from $L_{\rm SF,mean}$ (dashed black line in Fig. A1) to determine the completeness of the radio-excess selection in each bin.

Throughout the analysis in this paper, we have used a radio luminosity limit of $L_{150\,\rm MHz} \geq 10^{24}$ W Hz^{-1}, and performed the analysis for different AGN populations which have distinct radio luminosity functions. To derive appropriate completeness corrections as a function of SFR, we weight the completeness along the SFR axis by the radio luminosity function, down to 10^{24} W Hz^{-1} to derive

the radio-excess selection completeness corrections as a function of SFR for different AGN populations, which are shown in Fig. A2. The radio AGN luminosity functions are often modelled as a broken power law (e.g. Dunlop & Peacock 1990). Kondapally et al. (2022) fit the LERG luminosity function for the same sample that is used in this study, however they compute this over different redshift bins. We use the $0.5 < z \leq 1$ fit to the radio luminosity function from Kondapally et al. (2022) to compute the corrections (red solid line). Their luminosity function was found to be in good agreement with that of Best et al. (2014), and hence the good agreement seen with the corrections determined using the Best et al. (2014) LERG luminosity function (green dashed line). Kondapally et al. (2022) were not able to fit a model to the HERG luminosity function as the bright-end slope was largely unconstrained. Therefore, we use the $0.5 < z \leq 1$ best-fit HERG luminosity function from Best et al. (2014), given the good agreement between our measurements and their LERGs (orange dash dotted line). We find that the LERG luminosity functions do not evolve significantly between $z = 1$ and $z = 1.5$, and as a result, the derived completeness corrections are similar. We also compute a correction for the subset of LERGs hosted by SFGs (SF-LERGs). Although Kondapally et al. (2022) do not produce a fit to their SF-LERG luminosity functions, we use the difference in their fitted models to the total LERG and quiescent LERG luminosity functions to compute the SF-LERG corrections shown in Fig. A2 (blue dotted line).

In summary, we find that for the radio-excess selection criteria, we achieve a near 100 per cent completeness for SFR $<10\,\mathrm{M_{\odot}yr^{-1}}$, which can also be seen from the cross-over point in Fig. A1. At higher SFRs, the completeness falls quickly, but we note that the choice of the luminosity functions do not have a significant effect on the derived completeness corrections.

APPENDIX B: CHARACTERIZATION OF THE EFFECT OF SOURCE CLASSIFICATION UNCERTAINTIES

In this section, we assess the robustness of the SED-fitting based source classifications by using additional diagnostics that incorporate spectroscopic observations and X-ray observations.

B1 Spectral stacking of LERGs and HERGs

At the time of the first data release of LoTSS-Deep, the vast majority of the radio sources lacked spectroscopic data, which provide the most robust method of classifying different modes of AGN using emission line diagnostics. As a result, the source classifications used in this study (see Best et al. 2023) are based primarily on photometric SED fitting incorporating UV to X-ray data sets in order to identify features of radiatively efficient AGN activity (i.e. the HERGs) and separate these from radiatively inefficient AGN (i.e. the LERGs).

The recent Dark Energy Spectroscopic Instrument Early Data Release (DESI EDR; DESI Collaboration 2023) has provided spectroscopic observations for a moderate fraction (∼20 per cent) of the LOFAR detected sources in the ELAIS-N1 and Boötes fields. To test the robustness of the source classifications using these new spectroscopic observations, we construct stacked (median) spectra for each of the HERG, SF-LERG, Q-LERG, and the SFG populations, as identified based on the classifications from Best et al. (2023). The spectral stacking process used is presented and described in detail by Arnaudova et al. (2024). In summary, we first apply Galactic extinction corrections using Schlegel, Finkbeiner & Davis (1998) and the Milky Way reddening curve from Fitzpatrick (1999) with $R_{\mathrm{V}} = 3.1$, and then de-redshift the individual spectra and resample them on to a common wavelength grid. These are then normalized at the reddest possible end where data from all spectra is available (this also minimizes the effects of extinction). The stacked spectrum for each source type is then generated by computing the median in a given wavelength bin. The DESI selection function results in varying redshift distributions between each of the four samples; we hence limit the analysis to sources with spectroscopic redshifts in the range of $0.5 < z \leq 1$. To enable a more direct comparison to the results presented in the rest of the paper, we also only include sources with $L_{150\,\mathrm{MHz}} \geq 10^{24}\,\mathrm{W\,Hz^{-1}}$ when constructing the stacks.

The resulting stacked spectra for the HERGs, SF-LERGs, Q-LERGs, and SFGs are shown in Fig. B1. Where applicable, we mark key emission line features in the spectra, namely, [O II] λ3728, [Ne III] λ3870, Hβ, and [O III] λλ5007, 4959. The Q-LERG stack shows the Ca H and K absorption features, characteristic of the lack of young stars, along with a lack of emission line features that are typically indicative of star formation or (radiatively efficient) AGN activity; this is inline with the expectations of Q-LERGs being the jet-mode (i.e. radiatively inefficient) AGN population. The HERG stack shows strong emission from the [O III] line (35.12 eV), along with a weak detection of the higher ionization [Ne III] line (40.96 eV), both of which require the presence of a hard ionizing radiation field from an AGN. The presence of other features such as Hβ and the [O II] lines trace star formation activity (e.g. Kennicutt 1998) within the host galaxies of the HERGs. The strong [O III] emission seen for the HERGs, with a $\log_{10}([\mathrm{O\,III}]/\mathrm{H}\beta) = 1.0$, gives further indication of AGN activity. If the SF-LERGs are indeed radiatively inefficient AGN, like the Q-LERGs, but simply hosted in SFGs, we would expect the SF-LERG and SFG stack to present similar emission line features. Qualitatively, the SF-LERG stack is similar to the SFG stack, both showing stronger [O II] emission associated with star formation compared to [O III]. The $\log_{10}([\mathrm{O\,III}]/\mathrm{H}\beta)$ ratio for the SF-LERG stack is 0.7, which is lower than that of the HERGs, but higher than the value of 0.4 found for the SFG stack. Compared to the HERGs, the SF-LERGs also display a lower [O III]/[O II] ratio. Overall, these results suggest that while there may be a small level of contamination of SF-LERGs by low luminosity AGN, their average emission line features are broadly consistent with star formation activity.

We note that the above analysis presents an average view of each source type and could only be performed at present for a subset of the radio sources with spectroscopic data available. The use of emission line ratio diagnostics, such as the BPT classification or excitation index, provides the most robust method of classifying LERGs and HERGs (e.g. Best & Heckman 2012). Such an analysis requires the detection and measurement of at least 4–6 different emission lines, which are not always available for each source with DESI spectra, further reducing the number of sources for which such an analysis could be performed; we have therefore focused on performing spectral stacking in this paper. For the subset of radio sources detected within DESI EDR where emission lines can be measured robustly, such spectroscopic classifications will be presented in future work (Arnaudova et al., in preparation). Detailed spectroscopic classification for the vast majority of the radio sources will only be enabled by the upcoming WEAVE spectrograph (Jin et al. 2024), which will provide dedicated spectroscopic follow-up of LOFAR-detected sources, including *all* LOFAR-Deep sources as part of the WEAVE–LOFAR survey (Smith et al. 2016). This will overcome many of the limitations of existing SED-fitting based source classifications, including providing more reliable estimates of AGN bolometric luminosities and provide more robust redshifts.

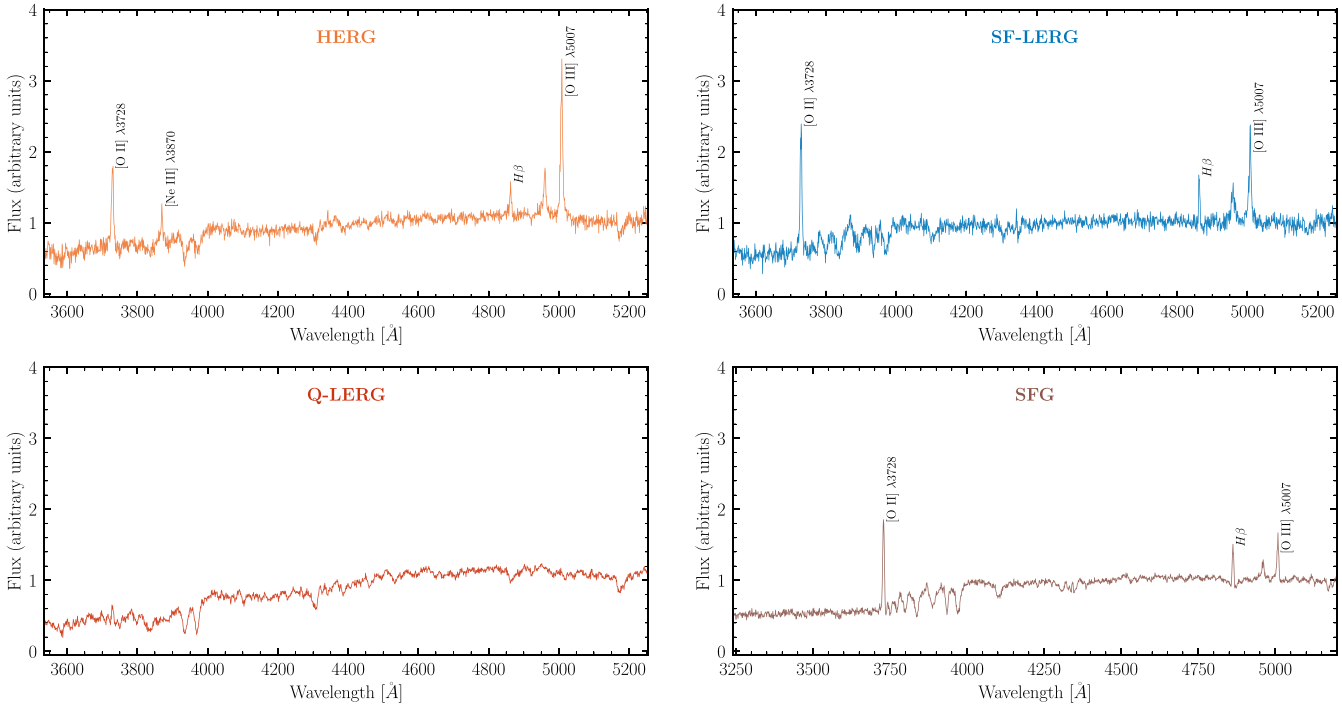

Figure B1. The median stacked spectra for HERGs, SF-LERGs, Q-LEGRs, and SFGs across $0.5 < z \leq 1$. The individual spectra, derived from the DESI EDR (DESI Collaboration 2023), are shifted to the rest frame, normalized and resampled on to a common wavelength grid before computing a median stacked spectrum. The Q-LERG stack shows Ca H and K absorption features, indicative of an old stellar population, with no signs of emission lines associated with either star formation or AGN activity. The HERG stack show strong detection of high-excitation emission lines, such as [Ne III] and [O III], and an [O III]/Hβ ratio associated with the presence of AGN activity.

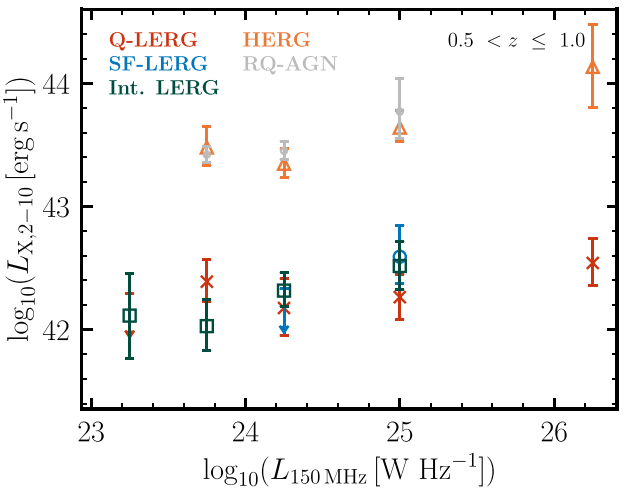

Figure B2. The median stacked 2–10 keV rest-frame X-ray luminosities as a function of radio luminosity for LERGs hosted by different galaxy types, HERGs, and RQ-AGN across $0.5 < z \leq 1$. The stacked X-ray luminosities represent the median X-ray luminosities based on bootstrap resampling, which are corrected for the contribution from XRBs. The uncertainties are computed using the corresponding bootstrap method. At a given radio luminosity, the LERGs, regardless of their host galaxy star formation activity, show over an order of magnitude lower X-ray luminosities than the HERGs or RQ-AGN.

We note that for the shallower but wider LoTSS-DR2 (Hardcastle et al. 2023), where large SDSS spectroscopic samples are available, the classification of LERGs and HERGs is now possible using a radio-excess selection and BPT classification (Drake et al. 2024). This analysis, which focuses primarily at lower redshifts ($z \lesssim 0.5$) has also found the existence of a considerable population (∼30 per cent) of LERGs hosted by SFGs. We expect this population to be less prevalent at lower redshifts but the fact that the use of the more robust emission line classifications still identifies a population of SF-LERGs suggests that these are not simply due to misclassifications from the SED fitting process.

B2 Average X-ray properties of LERGs and HERGs

To further test the robustness of the source classifications, we investigate the X-ray properties of radio-detected AGN. X-ray observations can be used to trace radiatively efficient (radiative mode) AGN. For this analysis, we focus on the Boötes deep field which has coverage from deep *Chandra* imaging over the full ∼9.6 deg^2 of the field as part of the the *Chandra* Deep Wide-Field Survey (CDWFS; Masini et al. 2020). The CDWFS covers 3.4 Ms worth of imaging data across the soft (0.5–2 keV), hard (2–7 keV), and the broad (0.5–7 keV) bands, reaching depths of 4.7×10^{-16}, 1.5×10^{-16}, and 9×10^{-16} erg cm^{-2} s^{-1}. In addition to the imaging data sets, Masini et al. (2020) also present a catalogue of 6891 X-ray detected sources across the three bands.

In addition to the LERGs (split into three subgroups based on their star formation activity) and the HERGs, we also investigate here the properties of the radio-quiet AGN (RQ-AGN), which are defined as sources that do not display a radio-excess but are identified as AGN based on SED fitting (see Best et al. 2023). Like the HERGs, the RQ-AGN are thought to be powered by radiatively efficient AGN, and their comparison to the LERGs can provide additional insights. Throughout this analysis, our aim is to understand the properties of the AGN as identified and classified based on the radio data; our

starting point is therefore the five classes of radio-detected AGN. We initially cross-match the radio-detected AGN with the Masini et al. (2020) X-ray catalogue (in the hard band), finding that around 33 per cent and 30 per cent of the HERGs and RQ-AGN, respectively, are also detected at X-ray wavelengths. In contrast, we find that only ∼2 per cent of the LERGs are X-ray detected (with the X-ray detections being split roughly equally amongst the three subgroups). The RQ-AGN and the HERGs are both expected to be powered by a radiative-mode AGN which emit strongly in the X-rays due to inverse-Compton scattering of photons from the black hole accretion disc; the considerable fraction of both RQ-AGN and HERGs that are X-ray detected is therefore expected. LERGs on the other hand are expected to be powered by radiatively inefficient accretion, which can explain the low X-ray detection rate. In addition, the similarly low X-ray detection fractions found for LERGs hosted within quiescent, intermediate, and SFGs indicates that the SF-LERGs are likely not misclassified radiative-mode AGN. It is possible that some of the X-ray emission from the X-ray detected LERGs is associated with the radio jets (e.g. Hardcastle 2009).

A significant fraction of our radio-detected AGN are however undetected in the X-rays; to gain a more complete understanding of the radio-detected AGN population, we perform an X-ray stacking analysis to compute the average X-ray luminosities of each group of AGN; the full details of this process will be described by Holc et al. (in preparation). To ensure that there are sufficient sources in each group of AGN, we focus our analysis within the redshift range $0.5 < z \leq 1$. Over this redshift range, we split each AGN sample into five radio luminosity bins and derived the stacked average X-ray luminosities in each bin. Using the positions of the radio-detected sources, we calculated the stacked count rates and fluxes using the hard band (2–7 keV) CDWFS images. We incorporated both the X-ray detections and non-detections into our stacking analysis as the detections constitute a significant fraction of the HERGs and RQ-AGN. To derive robust stacked X-ray luminosities and uncertainties, for each radio luminosity bin, we repeat this process 10 000 times by performing a bootstrap resampling of the input source list, to derive a distribution of 10 000 realizations of the average stacked X-ray fluxes. We took the median of this distribution as our best estimate of the stacked X-ray fluxes, with the corresponding 1σ uncertainties estimated using the 16th and 84th percentiles. The stacked X-ray fluxes were then converted to rest frame 2–10 keV X-ray luminosities using the mean redshift of the bin ($z_{\rm mean} = 0.75$) and assuming an X-ray power-law spectrum with a photon index of $\Gamma = 1.8$.

The X-ray emission from a galaxy can arise not just from AGN activity but also from X-ray binaries (XRBs), which has been found to be well correlated with the star formation activity (e.g. Lehmer et al. 2010; Mineo et al. 2014; Lehmer et al. 2016; Aird, Coil & Georgakakis 2017). We estimate the contribution to the X-ray luminosity from XRBs using the empirical scaling relationship found by Lehmer et al. (2016) and subtract this from our stacked values. The resulting stacked 2–10 keV rest-frame X-ray luminosity as a function of radio luminosity for different groups of AGN are shown in Fig. B2. At a fixed radio luminosity, we find that both HERGs and RQ-AGN show significantly higher average X-ray luminosities, by over an order of magnitude, compared to the LERGs. Moreover, at a given radio luminosity, the stacked X-ray luminosities for LERGs hosted by galaxies of different star formation activities are consistent with each other. These results suggest that LERGs within each of the quiescent, intermediate, and star-forming systems are not significantly contaminated on a population level by radiatively efficient AGN, which show much higher X-ray luminosities. The consistency between the HERGs and RQ-AGN provides further evidence that these are both powered by radiatively efficient AGN. As X-rays trace the accretion activity on to the black hole, we would expect that these significant differences in the X-ray luminosities will also result in significant differences in the average black hole accretion rates between the LERGs and HERGs. Further detailed analysis of the average black hole accretion rates, including an investigation of their trends with radio luminosity and other galaxy properties will be investigated in future work (Holc et al., in preparation).

This paper has been typeset from a TEX/LATEX file prepared by the author.